

Assessment of aeolian dust concentration, elemental composition, and their wet and dry deposition fluxes over the Northeast Arabian Sea

Suresh, K.^{1,2}, Udisha Singh^{1,3}, Ashish Kumar Jha⁴, Vishnu Murthy Matta⁵, A.K. Sudheer²,
Ashwini Kumar^{1,3*}

¹CSIR-National Institute of Oceanography, Dona Paula, Goa, India

²Physical Research Laboratory, Ahmedabad, India

³Academy of Scientific and Innovative Research (AcSIR), Ghaziabad, U.P., 201002- India

⁴Department of Zoology, Hislop College, Nagpur, 440001, (M.S), India

⁵The School of Earth, Ocean and Atmospheric Sciences, Goa University, Taleigao, India

*Corresponding author: Ashwini Kumar, Geological Oceanography Division
CSIR-National Institute of Oceanography, Dona Paula, Goa-403 004, India

E-mail: ashwinikumarjha@gmail.com, ashwinik@nio.org

Tel: +91 832 2450368, Fax: +91 832 2450602

Abstract:

Atmospheric aerosol over the Arabian Sea is significantly impacted by the long-range transported mineral dust from the surrounding continents. This transported mineral dust is hypothesized and tested during several studies to see the impacts on the surface ocean biogeochemical processes and subsequently to the Carbon cycle. It is, thus important to quantify dust contributions and their fluxes to the Arabian Sea. Here we assess temporal variability of dust concentration, their elemental characteristics as well as quantify their dry and wet deposition fluxes over the North-eastern Arabian Sea. The dust concentrations were found to vary from 59 to 132 $\mu\text{g m}^{-3}$ which accounts for 50 to 90% of total mass during dusty days. However, its contribution during pre and post dust storms ranges between 6 to 60%. Relatively higher dust dry deposition flux of $28 \pm 7 \text{ mg m}^{-2} \text{ day}^{-1}$ (range: 20-44) is estimated for dusty days compared to pre and post dusty days (range: 0.4 – 22 $\text{mg m}^{-2} \text{ day}^{-1}$). In contrast to dry deposition fluxes, significantly higher fluxes are estimated from wet deposition, averaging around $240 \pm 220 \text{ mg m}^{-2} \text{ day}^{-1}$. These values are five times higher than those reported from cruise samples collected over the Arabian Sea. The contribution of dust to aerosol mass is further ascertained using elemental composition, wherein a significant correlation was observed between Fe and Al ($r^2 = 0.77$) for samples collected during the dusty period, highlighting their similar crustal sources. Our estimation of dust flux over this region has implications for the supply of nutrients associated with natural dust to the surface water of the Arabian Sea.

Keywords: Aerosol; Mineral Dust; Trace Element; Deposition Flux; Arabian Sea

Introduction

Atmospheric mineral dust is one of the significant components in the earth's system that affects the radiation budget, biogeochemical cycles, and human health (Okin et al., 2004; Jickells et al., 2005; Mahowald et al., 2005). The absorbing and scattering properties of aerosols affect the earth's radiative budget (Tegen, 2003). Mineral dust also has an impact on the ecosystems, as it transports macro (inorganic and organic nitrogen) and micro-nutrients such as iron, phosphorus, and other trace metals (Duce et al., 1991; Jickells et al., 2005; Ramaswamy et al., 2017; Kumar et al., 2020; Li et al., 2021). The dust deposition supplies these nutrients, which have the potential to impact the primary productivity in surface waters (Jickells et al., 2005).

The Arabian Sea receive, one of the productive oceanic regions among the global oceans, has been identified as a perennial source of atmospheric CO₂ (Körtzinger et al. 1997; Sarma et al. 1998). It receives mineral dust as well as anthropogenic aerosols from the surrounding arid regions and highly polluted Indo-Gangetic plains in the Indian Sub-continent, respectively (Kumar et al., 2008, 2020; Ramaswamy et al., 2017; Kaskaoutis et al., 2018; Rashki et al. 2018, 2019; Aswini et al., 2020; Suresh et al., 2021a & b). The dust over the Arabian Sea also affects the rainfall intensity and the precipitation chemistry over this region (Das et al., 2015; Ramaswamy et al., 2017). The composition of dust derived from different sources to the Arabian Sea varies in different seasons, which is evident from their different geochemical characteristics (Kumar et al., 2020). The dry deposition in the Arabian Sea region from October to May is mostly dominated by the dust from the Arabian Peninsula and SW Asia (Iran, Afghanistan and Pakistan), while the wet deposition during the Southwest (SW) monsoon is dominated by the Arabian Peninsula and NE Africa (Kumar et al., 2020; Suresh et al., 2021). The dust storms are also a major reason for the exceedance of the aerosol concentration over the North-Eastern Arabian Sea (NEAS) in recent years (Agnihotri et al., 2015; Suresh et al., 2021b).

Several modelling studies have shown that mineral dust deposition plays an important role in primary productivity of the Arabian Sea, as absence of dust deposition would lower the productivity by 50% (Mahowald et al., 2005; Jickells et al., 2005; Guieu et al., 2019). Over the years, majority of work have highlighted dust contributions to the Arabian Sea from the Arabian Peninsula, SW Asia, and NE Africa to the Arabian Sea (Léon and Legrand, 2003; Aswini et al., 2020, Rashki et al., 2018; 2021). Although several studies have shown the influence of mineral dust on ocean biogeochemistry, studies pertaining with quantification of dust fluxes based on real time aerosol collection over the Arabian Sea are very sparse (Tindale and Pease, 1999; Kumar et al., 2008). Thus, our objective in this paper is to quantify wet and dry deposition fluxes over the northeastern Arabian Sea during the dust storm period and the SW monsoon season using the ground-based dry aerosol and wet deposition (rainwater) sample collection, respectively. We also aim to characterize dust aerosols collected from

wet and dry deposition using major element (Al, Fe, and Ti) composition and their ratios. We have further discussed their seasonal variability and factors affecting the flux. Thus, this study will be a valuable contribution to the aeolian research community and have significant implications towards the role of aeolian deposition to the surface water biogeochemical processes in the Arabian Sea.

1. Materials and methods:

1.1. Sampling description

Aerosol and rainwater samples were collected at a coastal station located on the northeastern Arabian Sea coast at the CSIR-National Institute of Oceanography, Goa, India (15.45° N, 73.80° E) (Figure 1). The sampling site is affected by seasonally reversing south west (SW) monsoon winds from June to September and north east (NE) monsoon winds from November to February. Apart from the two major monsoon wind systems, other regional and local winds in the dust source regions like the Summer Shamal winds, Levar winds, Red Sea winds, tropical cyclones and Western disturbance or Winter Shamal also play a major role in transporting the dust to the NEAS. A detailed meteorological setting over this region is described by Kumar et al., 2020 and Suresh et al., 2021a. In general, the major processes responsible for the aerosol deposition is either by dry deposition due to gravity and/or impact as well as by wet deposition due to in or below-cloud scavenging. Both dry and wet deposition aerosol samples were collected for the years 2012-2015.

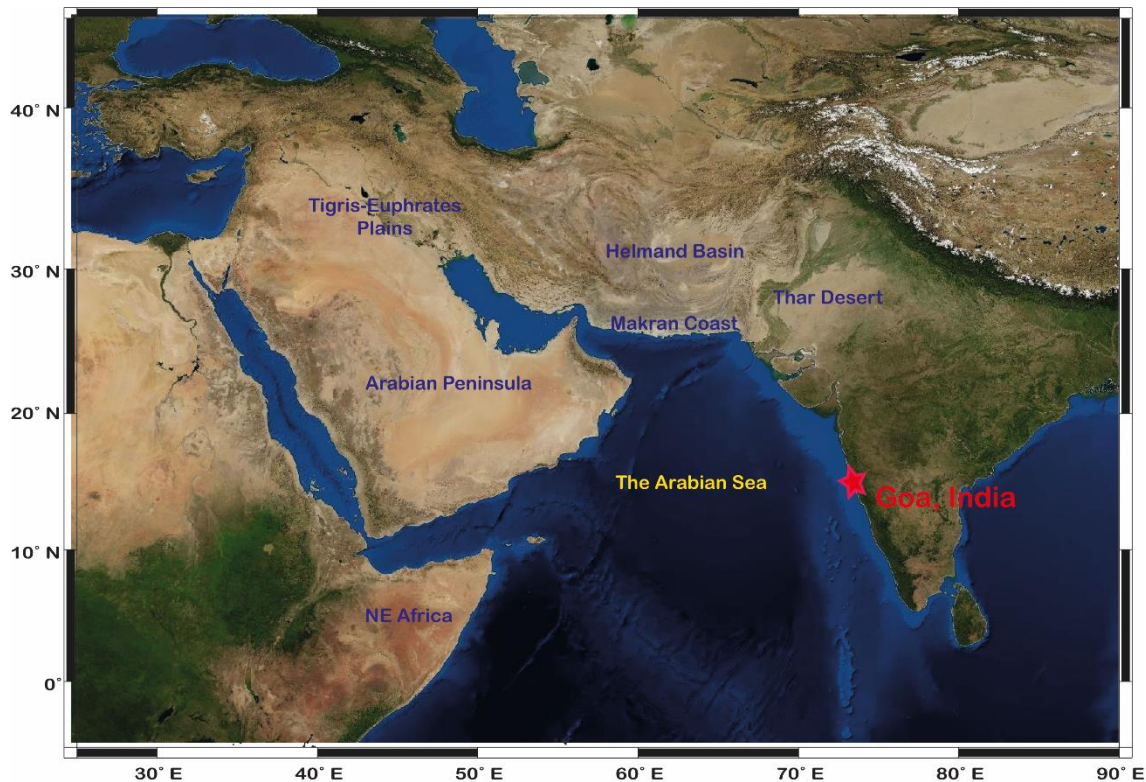


Figure 1: The sampling site Goa and the major dust sources to the Arabian Sea are labelled in the map.

1.1.1. Aerosol sampling

Aerosol samples were collected on a daily basis from 2012-2015 at the National Institute of Oceanography, Goa, India by using Envirotech High Volume Samplers (HVS) APM 430, with a flow rate of about $1\text{-}1.3\text{ m}^3\text{ min}^{-1}$ for a sample period of 22-24 hours. Typical cutoff aerodynamic diameter for collected particulate matter was less than 20 microns. GF/A glass fiber filters (20×25 cm sheets) (Whatman®) were used for the sampling. The filters were conditioned in an oven at 80°C and weighed before sampling. After the sampling, the filters were transferred and stored in Ziploc bags. Extreme care was taken while handling the filters to avoid any contamination or wear and tear. Several field blanks were collected by placing filters over the sampler for a few hours without running the pump. This was done to assess the level of contamination during sampling and storing of samples. The total suspended particulate (TSP) mass was calculated from the difference in the filter weight before and after sampling. During the monsoon season (June-September), no aerosol samples were collected due to the unavailability of dry days, as it rained almost every day at the sampling location. Most of the aerosols are removed due to scavenging by raindrops.

1.1.2. Wet deposition sample collection

Rainwater samples were collected in a plastic tray with a base area of 1 m^2 every rainy day during the SW rainy season from 2013 to 2015. The sample collecting trays were cleaned with utmost care using MQ water before and after sampling. After sample collection, the rainwater is filtered by using a pre cleaned (Milli-Q water) polycarbonate filter of $0.4\text{ }\mu\text{m}$ pore size to obtain the wet deposition particulates (WDP). The filtered WDP was dried at 40°C in an oven to remove water content and the weight of the samples was measured gravimetrically using a micro-balance. Further detailed information can be found in Suresh et al., 2021a. The samples were used for processing and analyses of geochemical tracers.

2.2 Sample preparation for chemical analysis

Crustal elements (Al, Ti, and Fe) were measured by digesting one-eighth portion of the filter ($\sim 54\text{ cm}^2$) for aerosol samples and 50 mg of WDP samples. There were 12 major dust storms identified based on the aerosol concentration, Aerosol Index (AI) and air mass back-trajectories (for back-trajectories refer supplementary material S2) (detail of identification of dust sources can be found in Kumar et al., 2020), that pass over the sampling station Goa for the years 2012-15, and a total of 69 aerosol filter samples were analyzed for the crustal elements (the sample details are given in Table.1 and 2). Sixteen wet deposited samples were selected for digestion for each of the three years 2013, 2014, and 2015 (one sample per week). Samples were digested in Savillex vial (15 mL capacity) with

0.5 mL HF and 3 mL HNO₃ at 110°C for 24 hours under a clean laminar flow bench. This process was continued until the samples were completely dissolved and then dried. Subsequently, all samples were made up to 50 mL with 2% supra-pure HNO₃ in pre-cleaned polypropylene bottles. Multiple field blanks, which were considered as procedural blanks during the analysis, were analysed for all crustal elements, and depending upon these blank concentrations, corrections were made in samples. The procedural blank concentration (including contribution from chemical reagents and filter blank) for Al, Fe and Ti are 0.05, 0.05, 0.04 µg m⁻³. Procedural blank concentrations for these elements are estimated by normalizing blank concentration to average air volume filtered (~1500 m³) for the study period. The crustal elements (Al, Fe, and Ti) concentrations were analyzed using ICP-OES (Agilent 710) at the National Institute of Oceanography, Goa. The concentration of all three elements in sample and blank filters were found more than the detection limit (0.05, 0.05 and 0.06 ppm for Al, Fe and Ti respectively) of each element measured using the ICP-OES. In addition to samples, a reference standard (NIST SRM 2710a) was also digested following similar procedure and elements were measured in this standard. Few samples and standards were analyzed repeatedly to determine the accuracy and precision of analysis; these replicate measurements show accuracy and analytical reproducibility of 10 % or less for all three major elements.

2.3 Aerosol concentration and flux

a) Aerosol concentration

Aerosol concentrations of total suspended particulates (TSP) were calculated by measuring the mass of the aerosol particles collected on the filter, normalized by the volume of air sampled. All filters were equilibrated with ambient temperature and relative humidity during their weighing. The mass of the TSP collected in the filter was measured gravimetrically. The weighing balance is calibrated periodically and the pressure, temperature, and relative humidity were maintained at appropriate conditions before weighing the filters.

b) Dry and wet deposition flux

Dry deposition fluxes (F_d) were calculated based on the concentration of aerosols (C) and the depositional velocity of the particles (V_d):

$$F_d = C \times V_d \quad \text{Equation (1)}$$

Depositional velocity of aerosol particles was calculated based on Stokes law:

$$V_d = \frac{\rho_p d^2 g}{18\eta} \quad \text{Equation (2)}$$

where ρ_p is the density difference of the dust particle to the air and the density of the dust is considered 2.6 g/cm^3 (Schepanski et al., 2009; Chen et al., 2011; Vasilatou et al., 2017), d is the aerodynamic diameter of the particle, g is the gravity acceleration (in m/s^2) constant and η is the viscosity of air (in $\text{kg m}^{-1}\cdot\text{s}^{-1}$). To measure the size distribution of the dust that reaches NEAS, the wet deposition samples of 2013 were analyzed by using the Laser Particle Size Analyzer. A mono-modal distribution was observed with a median diameter of $7.96 \text{ }\mu\text{m}$ (Fig. 2), which can be considered as “ d ”, the aerodynamic diameter of the dust particles to calculate settling velocity using the equation (3). Since dust particles are irregular in shape and the shape of the particles affects the drag force and settling velocity, the dynamic shape factor (χ) has been applied to the above equation. The dynamic shape

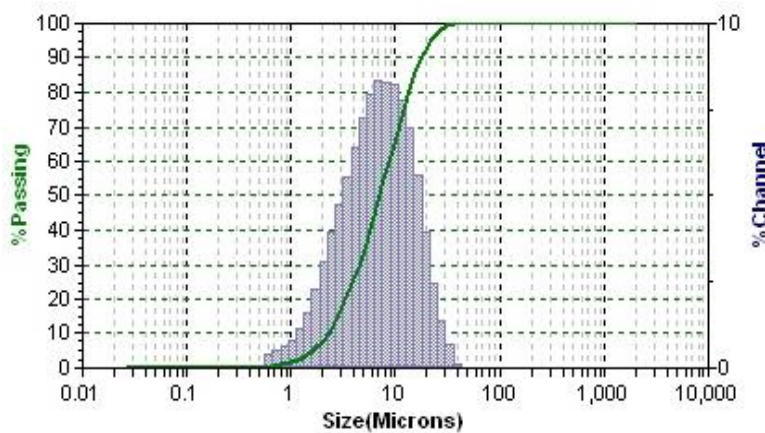


Figure. 2: The size distribution of wet deposited dust collected during SW monsoon of 2013.

factor of Quartz ($\chi=1.36$) (Davies 1979; Reid et al., 2003; Alexander et al., 2016) has been used in this study since the value for silicates is not available in the literature. So the depositional velocity of

dust particles after applying the dynamic shape factor becomes
$$V_d = \frac{\rho_p d^2 g}{18\eta\chi} \quad \text{Equation (3)}$$

This equation provides V_d of 335 m day^{-1} and fluxes for the dry deposition were calculated by using the equation (1). The settling velocity derived in this work is lower than those reported ($\sim 1000 \text{ m day}^{-1}$) by Shelley et al., (2015), Anderson et al., (2016) and Bergametti et al., (2018) in the eastern Atlantic station and western Africa region located close to the Saharan Desert. Also, while estimating the deposition velocity, several factors viz. wind friction velocity, turbulence and molecular diffusion, can impact on its calculation and introduce large uncertainty in its values (Bergametti et al., 2018). In this study, the estimated settling velocity is relatively low compared to those reported previously. In addition, the sampling site in this study is located far away (more than 1000 Km) from the source region which may result in transport of finer dust, thus the calculated V_d can be a better representative for this study.

The data on the Al concentrations in the samples were used to estimate the dust concentrations and fluxes for the aerosol samples by presuming that the Al in mineral dust is the same as in the Upper Continental Crust (UCC) (UCC with Al content of 8.04%; McLennan, 2001). It was reported that the wet deposited particles collected after filtration were mainly composed of mineral dust (Ramaswamy et al., 2017; Suresh et al., 2021b), which could provide an upper limit of dust flux.

2. Results and discussion

The details of the dust storm samples and the wet deposition samples collected are given in tables 1 and 2. The dust storms over the NEAS are more frequent in the summer than in the winter season (Kumar et al., 2020). Aerosol samples were collected for dust concentration in the twelve dust storms that reached the sampling station (Goa). The dust deposition flux of the twelve major dust storms (details given in table 1) has been calculated. The wet deposition flux has been calculated directly by measuring the weight of the particulates collected from the rainwater (2013-2015) since these particles form the total aeolian flux.

3.1 Aerosol concentrations over the eastern Arabian Sea:

The aerosol concentration over Goa for the years 2012-15 ranges from 1 to 356 $\mu\text{g m}^{-3}$ (Figure 3) with an average of 101 $\mu\text{g m}^{-3}$, the majority of the maximum aerosol concentration are observed during the passage of dust storms over the NEAS. The average aerosol concentrations during the study period are higher than the average aerosol concentrations ($80.9 \pm 29.5 \mu\text{g m}^{-3}$; Agnihotri et. al., 2015) measured at this site from December 2009 to January 2011. The seasonal variability in dry deposited samples is assessed by classifying months into two seasons viz. summer (April and May) and winter (October-March). However, only WDP was collected during the monsoon period (June-September). For logistic reasons, TSP samples were not collected during May 2012, December 2014, and the post-monsoon period of 2015 (October – December). During summer, the aerosol concentration for the period 2012-15 varied significantly from 1-356 $\mu\text{g/m}^3$ (average $92 \pm 54 \mu\text{g/m}^3$), while during the winter period the concentration varied between 2-298 $\mu\text{g/m}^3$ (average $102 \pm 49 \mu\text{g/m}^3$). The aerosol concentration during the post-monsoon period varied between 13-208 $\mu\text{g/m}^3$ (average $79 \pm 34 \mu\text{g/m}^3$).

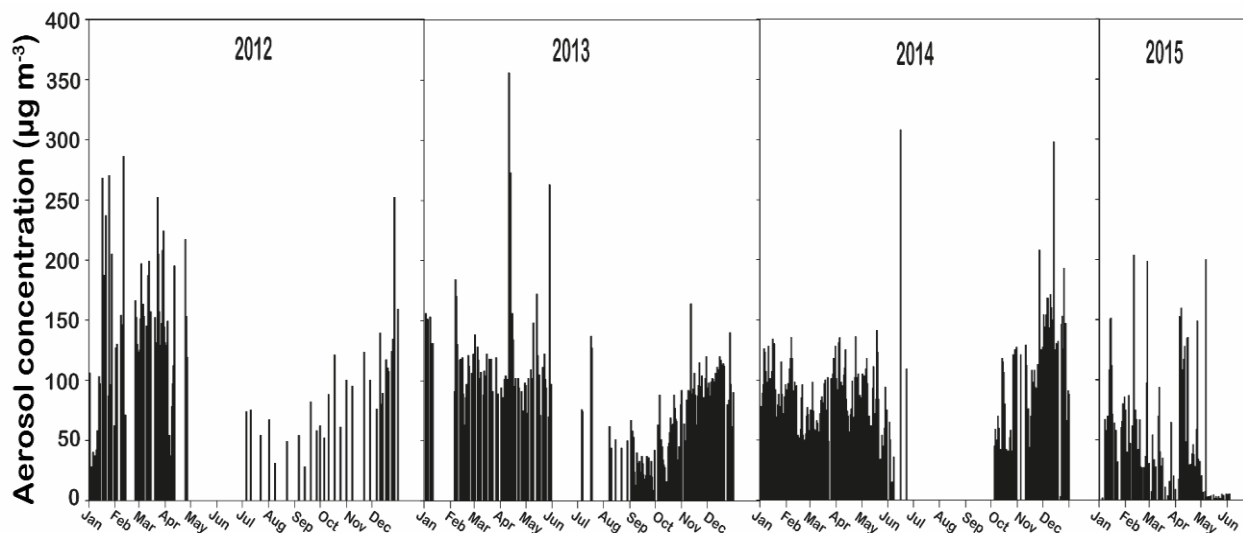
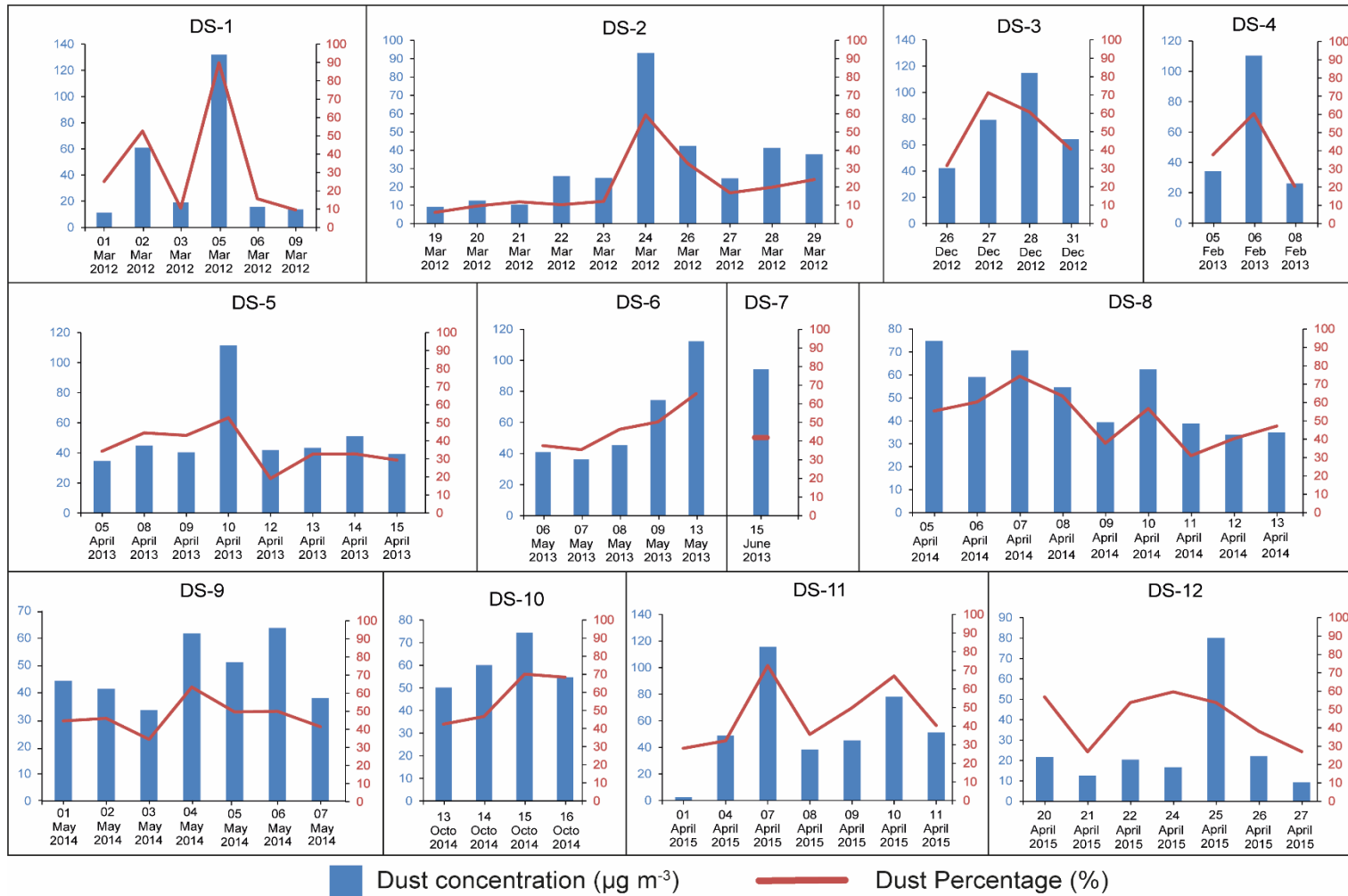


Figure 3: The aerosol concentrations over the eastern Arabian Sea for the years 2012 to 2015 (x-axis given in months). The maximum concentrations were observed during the dust storm events. The gap between the bars are the days with no sampling. There was no sampling between June to October (SW monsoon season).

3.2 Dust percentage in total aerosol concentration

Figure 4: The dust concentration (blue bars) for the twelve dust storm periods along with their dust percentages (red solid line) over the total aerosol concentration. Left hand y-axis is dust concentration right hand y-axis is dust percentage of total aerosol load. Most of the dust storm samples have dust concentrations of more than 50% (except DS-7) of the total aerosol concentration, showing the influence of the dust storms in the aerosol concentrations.



The dust concentrations and dust percentage show an increasing trend from the samples collected before dust storm and highest when the dust storm was passed over the sampling site and then decreases after waning of dust storm, indicating the influence of the dust storms on total dust concentrations at the sampling site (Figure 4). Dust concentrations vary greatly during the dust storm days, ranging from 60-132 $\mu\text{g m}^{-3}$ (Table 1) with an average of $85\pm 22 \mu\text{g m}^{-3}$. The dust concentrations observed during winter and summer dust storms averaged around $91\pm 24 \mu\text{g m}^{-3}$ and $81\pm 20 \mu\text{g m}^{-3}$, respectively. Based on this observation, it is difficult to conclude the role of the proximity of dust source region in playing any role in dust concentration over the NEAS. Nevertheless, relatively higher dust is seen in winter when the SW Asia (relatively proximal to our study site) is dominant source compared to summer when the Arabian Peninsula is dominant (See Supplementary material S2 for back-trajectories) (Kumar et al., 2020). This seasonal variability in the dust sources is important in understanding the influence of the different dust sources at different times of the year. The dust contribution to the total aerosol mass concentrations is relatively higher for the dust storm days (41 to 90% with an average of $60\pm 11\%$) (Figure 4), whereas it is relatively low for the pre and post dust storm samples ($32\pm 14\%$). The dust storm DS-7 was collected during the SW monsoon of 2013 when there was a monsoon break (no rain for 3-4 days) and the dust contribution to the total aerosol concentration was 41% which is lower than the average dust contribution. The reason for the low dust contribution during the monsoon is attributed to the high altitude transport of dust during this period (Ramaswamy et al., 2017) in comparison to those during dry period (Kumar et al., 2020). Due to strong monsoon winds, aerosols in the lower altitudes are typically dominated by sea-salt. The average dust percentages in the dust storm samples are much higher than the dust percentages measured in the Arabian Sea ($44\pm 15\%$) reported by Kumar et al., 2008. The dust percentages for the winter dust storms (excluding pre and post dust storm samples) (average = $67\pm 13\%$) are higher than the summer dust storms (average = $58\pm 9\%$), however the average dust percentage for the pre and post dust storm samples of winter (average = $67\pm 13\%$) is lower than the summer. It shows that the summer season in the NEAS is dustier than the winter period. Although some of the normal day's samples have shown high dust percentages, their aerosol concentrations were too low to be considered as dust storm samples (Table 2).

3.3 Dry and wet deposition dust fluxes over the eastern Arabian Sea

The aerosol dry deposition fluxes for the samples analyzed during the pre, post, and dust storm samples show a large variation, ranging from 1-44 $\text{mg m}^{-2} \text{day}^{-1}$ (Figure 5). The highest dust flux ($44 \text{mg m}^{-2} \text{day}^{-1}$) was measured during the dust storm of 05 March 2012 which originated from the Helmand basin of SW Asia (indicated by back trajectory analyses; Supplementary Figure S2) (Kumar

et al., 2020). The dust flux for the pre and post dust storm samples shows a large variation with a minimum of $1 \text{ mg m}^{-2} \text{ day}^{-1}$ to a maximum of $22 \text{ mg m}^{-2} \text{ day}^{-1}$ (average = $11 \pm 5 \text{ mg m}^{-2} \text{ day}^{-1}$). The dry deposition flux of the dust storm days varied from $20 - 44 \text{ mg m}^{-2} \text{ day}^{-1}$ (average of $28 \pm 7 \text{ mg m}^{-2} \text{ day}^{-1}$) (Figure 5), the dust flux during the dust storm samples is twice that of the pre and post-storm samples, indicating the role of the dust storm in the deposition flux of dust to the Arabian Sea during the dry seasons.

Out of the twelve dust storms observed during the study period, relatively higher dust fluxes were witnessed during the summer period, except for the year 2012, during which no dust storms were observed in the summer. The dust flux for the summer period varied from 189 to $272 \text{ mg m}^{-2} \text{ day}^{-1}$ with a total flux of 729 mg m^{-2} , whereas the dust flux in the winter period varied from 57 to $272 \text{ mg m}^{-2} \text{ day}^{-1}$ with the total flux of 431 mg m^{-2} (Figure 5). The higher dust flux during the summer season is mainly because of the greater number of dust storms that move towards the NEAS.

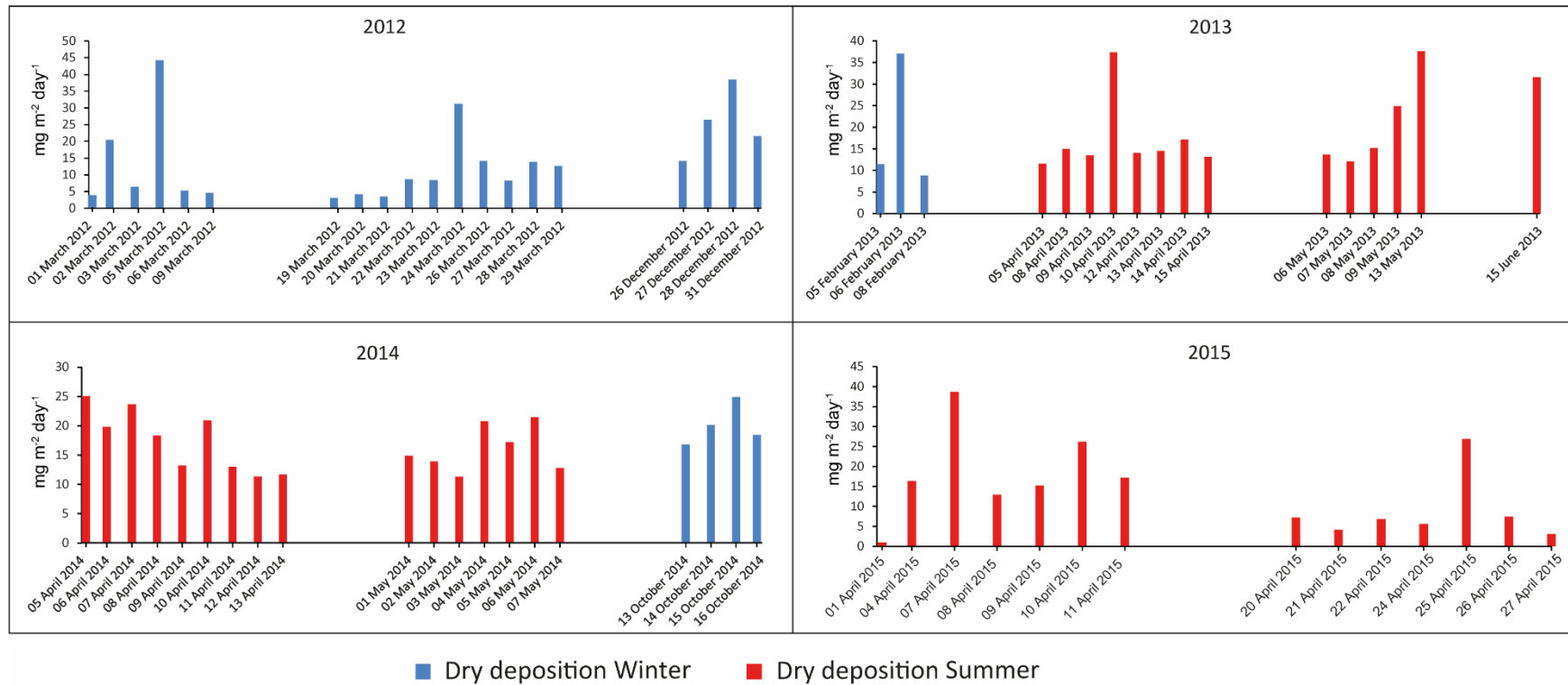


Figure 5. Dry deposition flux ($\text{mg m}^{-2} \text{day}^{-1}$) for the twelve dust storms observed for the years 2012 to 2015. The samples collected before during and post the dust plume pass over the NEAS are given. In most of the samples, the dust deposition during the dust storm periods is high when the dust plumes pass over NEAS. Blue and Red bars represent the dry deposition flux during winter and summer respectively.

The wet deposition fluxes during the SW monsoon for the years 2013 to 2015 ranged from 8 to 1089 mg m⁻² day⁻¹ (Table-3), with an average of 240±220 mg m⁻² day⁻¹. During the SW monsoon, it rains almost every day in the sampling station (Goa) (Ramaswamy et al., 2017) and the wet deposition is the dominant process for dust removal during SW monsoon season in this region (peninsular India). The three-year average flux for the beginning of the monsoon is 215±226 mg m⁻² day⁻¹ which increases to an average of 282±220 mg m⁻² day⁻¹ in the middle of the monsoon (during July and August). At the end of the monsoon, the average deposition flux decreased to 98±95 mg m⁻² day⁻¹. This trend in the deposition flux is mainly due to the decrease in the rainfall and the availability of dust-bearing winds, which change from the beginning to the end of monsoon (Suresh et al., 2021a), that supply a large amount of dust to the Arabian Sea during the SW monsoon period. Also, one of the reasons for this clear trend in the wet deposition flux is due to the steady flow of the wind systems such as the SW monsoon winds, summer shamal winds, the red Sea winds, and the Levar winds (Ramaswamy et al., 2017). The dust-carrying winds viz. Shamal winds and the Red Sea winds are more active during the beginning and middle of the monsoon, in comparison to the end of the monsoon period. The wind intensity, availability of dust-bearing winds play a major role in the wet deposition fluxes in this region. The average wet deposition fluxes for the years 2013 to 2015 are about eight to ten times higher than the dry deposition fluxes, which highlights the importance of wet deposition in this region. Also, it has to be noted that the aerosol dust flux reported in this study is only for the twelve dust storm periods, during which the dust and aerosol concentrations are high. In comparison, during the SW monsoon season, the dust emission is continuous (Suresh et al., 2021; Ramaswamy et al., 2017) and the wet deposited particulates were collected for all the rainy days (Figure 6).

From the above discussion, it is evident that the wet deposition fluxes are significantly higher than the dry deposition fluxes over the study region. We further compared our deposition flux data reported from other coastal, marine as well as continental locations. Very high deposition flux values (average = 6380 g m⁻² d⁻¹) have been reported by Hamza et al., (2011), from a coastal location in the UAE, which is in close proximity to the dust source region. In contrast, very low flux values (0.66 mg m⁻² day⁻¹) have been reported from a remote location of Kerguelen Island in the Southern Ocean (Heimbürger et al. 2013). The dust flux in this study is very low compared with the UAE (which is one of the major dust source regions), however, very low as compared to those observed at Kerguelen Island. These observations indicate the importance of favourable meteorological conditions, particularly the wind speed and direction, in controlling the dust flux in the NEAS. The spatial variation of dust flux over the marine region is well demonstrated by Vincent et al. (2016), which reported large variability in dust flux from east to west with higher flux in the east (4.2-100 g m⁻² year⁻¹) in contrast

to the west (2.2 to $16 \text{ g m}^{-2} \text{ year}^{-1}$). Such variability is attributed to the wind pattern and intensity as well as the proximity of dust sources to the sampling location. Vincent et al. (2016) have also highlighted higher wet deposition fluxes as compared to dry deposition fluxes, similar to our study.

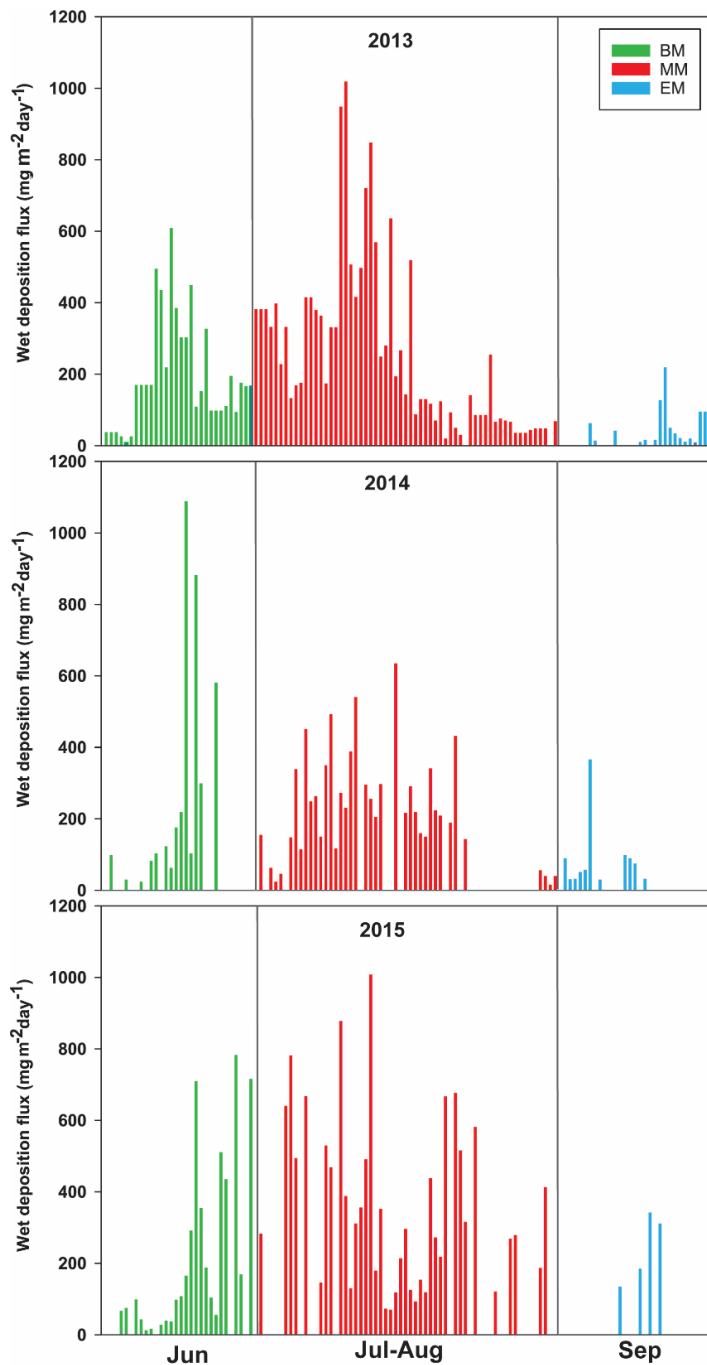


Figure 6: Wet deposition flux ($\text{mg m}^{-2} \text{ day}^{-1}$) for the years 2013, 2014, and 2015. The monsoon season is divided into beginning (BM), mid (MM) and end of the monsoon (EM). The wet deposition is high during the mid of monsoon period, and low during the end of the monsoon. The rainfall is high and the dust-bearing winds like summer shamal winds and the Red sea winds are active during the mid monsoon period affects the wet deposition flux.

3.4 Elemental composition of the dust:

To characterize the aerosols over the NEAS, crustal elements viz. Al, Fe, and Ti were measured in aerosol samples collected before, during and post-dust storm days. The elemental ratios for the major dust storms and wet deposition of 2013 were already reported by Kumar et al., 2020 and Suresh et al., 2021a, and in this study, we try to compare them with the pre and post dust storm samples. It is to be noted that Kumar et al., 2020 have not measured Ti in the dust storm samples, and only Fe/Al is compared with the pre and post dust storm samples in that work. The Fe was found to correlate significantly ($r^2 = 0.77$; Figure. 7a) with Al in the dust storm samples reported by Kumar et al., 2020, which were used as a tracer for crustal contribution in the aerosol compositions indicating their crustal origin (Kumar and Sarin, 2009; Kumar et al., 2020 and Suresh et al., 2021a). The Fe and Ti concentrations for the pre and post dust storm samples varied from 0.11 to 9.18 $\mu\text{g m}^{-3}$ with an average of $2.8 \pm 1.2 \mu\text{g m}^{-3}$ for Fe and 0.02 to 1.87 $\mu\text{g m}^{-3}$ with an average of $0.38 \pm 0.33 \mu\text{g m}^{-3}$ for Ti. The Fe/Al ratio varied from 0.11 to 4.40 ($A_v = 0.77$; $SD = 0.79$) for the pre and post dust storm samples, whereas Fe/Al for the dust storm samples varied from 0.28 to 0.66 ($A_v = 0.44$; $SD = 0.10$). The average Fe/Al ratio of the dust storm samples is similar to the UCC of 0.44 (Taylor and McLennan, 1985) indicating that these dust storm samples are mainly derived from the lithogenic fraction.

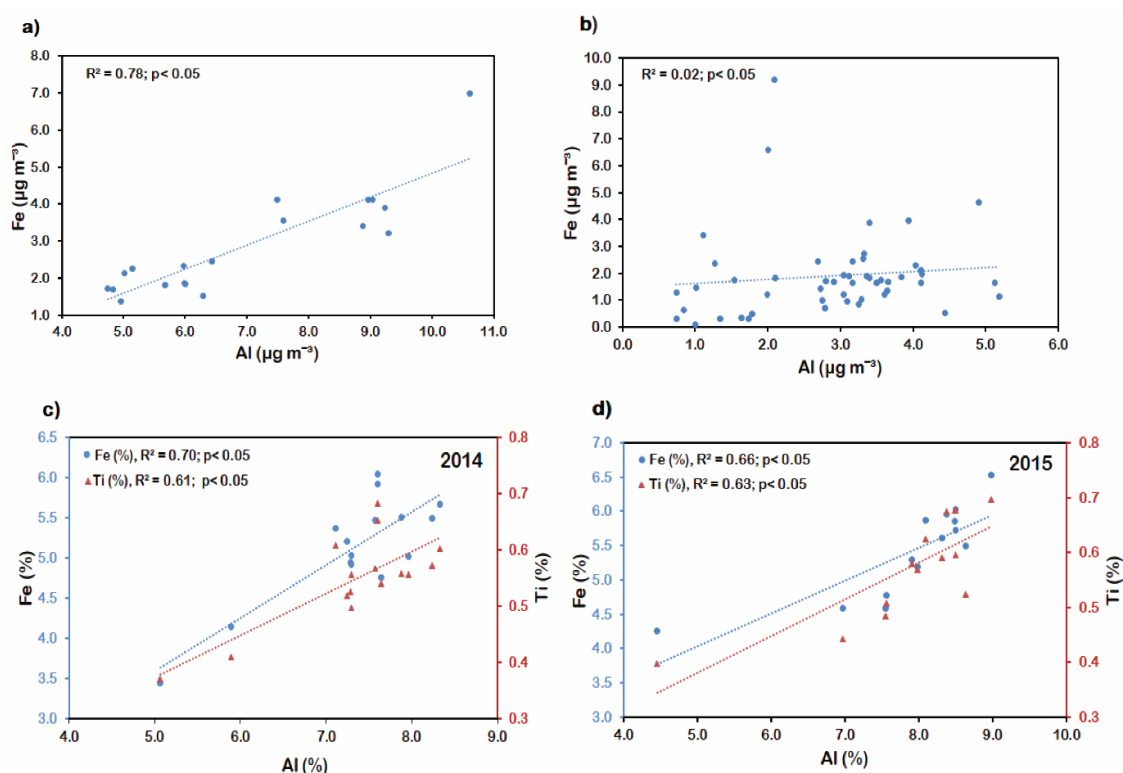


Figure 7: The scatter plots showing correlation analysis of Fe vs Al for the dust storm (a) and pre and post dust storm samples (b). Plots (c) and (d) show the Fe Vs Al and Ti Vs Al for the wet deposition samples of 2014 and 2015 respectively. The data points given as square boxes (d) are not taken for correlation calculation.

The Ti/Al ratio varied from 0.03 to 0.9 ($A_v = 0.14$; $SD = 0.14$). The pre and post dust storm samples shows very poor correlation for Fe/Al and Ti/Al ($r^2 = 0.016$; $r^2 = 0.091$ respectively Figure. 7b), suggesting contribution from the non-crustal sources. Since most of the dry deposited aerosol samples were collected during the pre and post-monsoon period, the aerosol samples might be impacted from the anthropogenic aerosols from local sources as well as those transported from the Indo-Gangetic plains towards the Arabian Sea (Kaushik et al., 2021).

The elemental composition (Fe, Al and Ti) of dust measured in wet deposited dust for the three year are provided in Table-3. Wet deposited samples for the 2014 and 2015 monsoon months show a relatively homogeneous Fe/Al ratio with an average of 0.70 and 0.72 for 2014 and 2015, respectively. All the wet deposited samples show enriched Fe/Al from the UCC value (0.44; Taylor and McLennan, 1985; McLennan, 2001), which may be due to the dust contribution during the SW monsoon season from the NE African sources which are abundant in Fe-rich basalts. Similarly, Ti/Al ratios did not exhibit any significant temporal variability, with an average ratio of 0.07 for both 2014 and 2015 samples. These ratios are well within the range of the value given by Suresh et al., 2021 for the wet deposited samples of 2013. Also, the correlation between Fe, Ti to Al of the wet deposited samples of 2014 and 2015 (Fe/Al= 0.70 and 0.76; Ti/Al= 0.60 and 0.71) are similar to the 2013 samples (Fe/Al= 0.75 and Ti/Al= 0.66) reported by Suresh et al., 2021. The Fe and Ti correlate well with Al for the wet deposited samples, indicating a similar origin and clearly highlighting the dominance of dust in the wet particulate matter. Although the non-dust storm aerosol samples were also enriched in Fe than the UCC like the wet deposited samples, their poor correlation with Al shows the non-crustal origin indicating that natural dust is not the only source for Fe, Ti and Al during non-dusty periods (Kumar et al., 2010).

4 Summary

In this study, the dust concentration, their dry and wet deposition fluxes were estimated for the twelve dust storms events (pre, post and during) that reached the NEAS (2012-2015) and those collected during the SW monsoon season of the years 2013-2015. The collected dust samples (wet and dry) were characterized using major elements (Al, Fe, and Ti) and their ratios. Further, we have assessed long-term seasonal variability in dust fluxes as well as their elemental characteristics.

The dust storms towards the NEAS are more frequent during the summer season (April and May) than the winter season (October to March) during the study period, and most of these dust storms are mainly influenced by the western disturbances. The dust deposition is also higher during the summer months than the winter months for all the dust storms that reached the NEAS. The wet deposition

occurs mostly during the SW monsoon period (June to September) and the dust deposition for the three years 2013, 2014, and 2015 are 208, 204, and 308 mg m⁻² day⁻¹ respectively. The wet deposition flux is maximum at the middle of the monsoon and minimum at the end of the monsoon. The favourable wind pattern as well as high winds in the source regions play a major role in the wet deposition fluxes in this region. Also, the wet deposition fluxes were significantly higher than the dry deposition fluxes. The non-dust storm samples show large variability in Fe/Al values as compared to dusty day samples (which average around UCC values) suggesting the influence of non-crustal sources during the pre and post dust storm period. Relatively enriched Fe/Al ratios (from UCC) were observed for wet deposited samples for all three years, however, a very significant correlation between Fe and Al was observed for these samples. This suggests the dominance of crustal sources with characteristics different Fe/Al compositions.

The reported long-term data on dust fluxes, their elemental characteristics and associated seasonal variability at a regional scale are important to constrain the supply of nutrients to the Arabian Sea and have implication for the better understanding of surface water biogeochemical processes.

Acknowledgment

Financial support for this research is by CSIR Project GEOSINK and CLICNIO (MLP1802). A.K. thank the Department of Science and Technology, Govt. of India, for providing partial financial support under the INSPIRE Faculty scheme; IFA13-EAS-13 and SPLICE Program (Grant DST/CCP/Aerosol/85/2017(G)). Also, the researchers K. Suresh and Udisha Singh are thankful to the Department of Science and Technology for the funding through INSPIRE Research Fellowship (IF140405) and (IF180350). The authors gratefully acknowledge the NOAA Air Resources Laboratory (ARL) for the provision of the HYSPLIT transport and dispersion model (<http://www.ready.noaa.gov>). We thank Robin John for help during the analyses of major elements in aerosol samples using ICP-OES.

Data Availability Statement: The authors confirm that the data supporting the findings of this study are available within the article as Table 1-3.

References:

Agnihotri, R., Karapurkar, S. G., Sarma, V. V., Yadav, K., Kumar, M. D., Sharma, C., & Prasad, M. V. S. N. (2015). Stable isotopic and chemical characteristics of bulk aerosols during winter and summer Seasons at a station in western coast of India (Goa). *Aerosol and air quality research*, 15(3), 888-900.

- Alexander, J. M., Bell, D. M., Imre, D., Kleiber, P. D., Grassian, V. H., & Zelenyuk, A. (2016). Measurement of size-dependent dynamic shape factors of quartz particles in two flow regimes. *Aerosol Science and Technology*, 50(8), 870-879.
- Anderson, R. F., Cheng, H., Edwards, R. L., Fleisher, M. Q., Hayes, C. T., Huang, K. F., & Lu, Y. (2016). How well can we quantify dust deposition to the ocean? *Philosophical Transactions of the Royal Society A: Mathematical, Physical and Engineering Sciences*, 374(2081), 20150285.
- Aswini, M.A., Kumar, A., Das, S.K., 2020. Quantification of long-range transported Aeolian dust towards the Indian peninsular region using satellite and ground-based data-a case study during a dust storm over the Arabian Sea. *Atmos. Res.* 239, 104910.
- Bergametti, G., Marticorena, B., Rajot, J. L., Foret, G., Alfaro, S. C., & Laurent, B. (2018). Size-Resolved Dry Deposition Velocities of Dust Particles: In Situ Measurements and Parameterizations Testing. *Journal of Geophysical Research: Atmospheres*, 123(19), 11-080.
- Chen, J., & Li, G. (2011). Geochemical studies on the source region of Asian dust. *Science China Earth Sciences*, 54(9), 1279-1301.
- Das, S., Dey, S., Dash, S.K., Giuliani, G., Solmon, F., 2015. Dust aerosol feedback on the Indian summer monsoon: Sensitivity to absorption property. *J. Geophys. Res.-Atmos.* 120 (18), 9642–9652.
- Davies, C. N. (1979). Particle-fluid interaction. *Journal of Aerosol Science*, 10(5), 477-513.
- Duce, R. A., & Tindale, N. W. (1991). Atmospheric transport of iron and its deposition in the ocean. *Limnology and oceanography*, 36(8), 1715-1726.
- Guieu, C., Al Azhar, M., Aumont, O., Mahowald, N., L'evy, M., Eth'e, C., Lachkar, Z., 2019. Major impact of dust deposition on the productivity of the Arabian Sea. *Geophys. Res. Lett.* 46 (12), 6736–6744.
- Hamza W, Enan MR, Al-Hassini H, Stuut JB, De-Beer D (2011) Dust storms over the Arabian Gulf: a possible indicator of climate changes consequences. *Aquat Ecosyst Health Manag* 14(3):260–268
- Heimbürger A, Losno R, Triquet S (2013) Solubility of iron and other trace elements in rainwater collected on the Kerguelen Islands (South Indian Ocean). *Biogeosciences* 10(10):6617–6628
- Jickells, T. D., An, Z. S., Andersen, K. K., Baker, A. R., Bergametti, G., Brooks, N., & Kawahata, H. (2005). Global iron connections between desert dust, ocean biogeochemistry, and climate. *Science*, 308(5718), 67-71.
- Kaskaoutis, D. G., Houssos, E. E., Solmon, F., Legrand, M., Rashki, A., Dumka, U. C., ... & Singh, R. P. (2018). Impact of atmospheric circulation types on southwest Asian dust and Indian summer monsoon rainfall. *Atmospheric Research*, 201, 189-205.
- Körtzinger, A., Duinker, J. C., & Mintrop, L. (1997). Strong CO₂ emissions from the Arabian Sea during south-west monsoon. *Geophysical Research Letters*, 24(14), 1763-1766.
- Kumar, A., Sarin, M.M., Sudheer, A.K., 2008. Mineral and anthropogenic aerosols in Arabian Sea-atmospheric boundary layer: sources and spatial variability. *Atmos. Environ.* 42 (21), 5169–5181.

- Kumar, A., & Sarin, M. M. (2009). Mineral aerosols from western India: temporal variability of coarse and fine atmospheric dust and elemental characteristics. *Atmospheric Environment*, 43(26), 4005-4013.
- Kumar, A.; Sarin, M. M.; Srinivas, B. Aerosol iron solubility over Bay of Bengal: Role of anthropogenic sources and chemical processing. *Mar. Chem.* 2010 Aug 20, 121, 167–175.
- Kumar, A., Suresh, K., Rahman, W., 2020. Geochemical characterization of modern Aeolian dust over the Northeastern Arabian Sea: Implication for dust transport in the Arabian Sea. *Sci. Total Environ.* 138576.
- Léon, J.F., Legrand, M., 2003. Mineral dust sources in the surroundings of the North Indian Ocean. *Geophys. Res. Lett.* 30 (6).
- Li, Y., Randerson, J. T., Mahowald, N. M., & Lawrence, P. J. (2021). Deforestation strengthens atmospheric transport of mineral dust and phosphorus from North Africa to the Amazon. *Journal of Climate*, 34(15), 6087-6096.
- Mahowald, N. M., Baker, A. R., Bergametti, G., Brooks, N., Duce, R. A., Jickells, T. D., Kubilay, N., Prospero, J. M., and Tegen, I.: Atmospheric global dust cycle and iron inputs to the ocean, *Global Biogeochem. Cy*, 19, GB4025, doi:10.1029/2004GB002402, 2005
- McLennan, S. M. (2001). Relationships between the trace element composition of sedimentary rocks and upper continental crust. *Geochemistry, Geophysics, Geosystems*, 2(4).
- Okin, G. S., Mahowald, N., Chadwick, O. A., & Artaxo, P. (2004). Impact of desert dust on the biogeochemistry of phosphorus in terrestrial ecosystems. *Global Biogeochemical Cycles*, 18(2).
- Ramaswamy, V., Muraleedharan, P. M., & Babu, C. P. (2017). Mid-troposphere transport of Middle-East dust over the Arabian Sea and its effect on rainwater composition and sensitive ecosystems over India. *Scientific reports*, 7(1), 13676.
- Rashki, A., Kaskaoutis, D. G., & Sepehr, A. (2018). Statistical evaluation of the dust events at selected stations in Southwest Asia: From the Caspian Sea to the Arabian Sea. *Catena*, 165, 590-603.
- Rashki, A., Kaskaoutis, D. G., Mofidi, A., Minvielle, F., Chiapello, I., Legrand, M., & Francois, P. (2019). Effects of Monsoon, Shamal and Levar winds on dust accumulation over the Arabian Sea during summer–The July 2016 case. *Aeolian Research*, 36, 27-44.
- Rashki, A., Middleton, N. J., & Goudie, A. S. (2021). Dust storms in Iran–Distribution, causes, frequencies and impacts. *Aeolian Research*, 48, 100655.
- Reid, J. S., Jonsson, H. H., Maring, H. B., Smirnov, A., Savoie, D. L., Cliff, S. S., ... & Tsay, S. C. (2003). Comparison of size and morphological measurements of coarse mode dust particles from Africa. *Journal of Geophysical Research: Atmospheres*, 108(D19).
- Sarma, V. V. S. S., Kumar, M. D., & George, M. D. (1998). The central and eastern Arabian Sea as a perennial source of atmospheric carbon dioxide. *Tellus B: Chemical and Physical Meteorology*, 50(2), 179-184.
- Schepanski, K., Tegen, I., & Macke, A. (2009). Saharan dust transport and deposition towards the tropical northern Atlantic. *Atmospheric Chemistry and Physics*, 9(4), 1173-1189.

- Shelley, R. U., Morton, P. L., & Landing, W. M. (2015). Elemental ratios and enrichment factors in aerosols from the US-GEOTRACES North Atlantic transects. *Deep Sea Research Part II: Topical Studies in Oceanography*, 116, 262-272.
- Suresh, K., Kumar, A., Ramaswamy, V., & Babu, C. P. (2021b). Seasonal variability in aeolian dust deposition fluxes and their mineralogical composition over the Northeastern Arabian Sea. *International Journal of Environmental Science and Technology*, 1-14.
- Suresh, K., Singh, U., Kumar, A., Karri, D., Peketi, A., & Ramaswamy, V. (2021a). Provenance tracing of long-range transported dust over the Northeastern Arabian Sea during the southwest monsoon. *Atmospheric Research*, 250, 105377.
- Taylor, S.R., McLennan, S.M., 1985. *The Continental Crust: Its Composition and Evolution*. Blackwell, Oxford, p. 312.
- Tegen, I.: Modeling the mineral dust aerosol cycle in the climate system, *Quaternary Sci. Rev.*, 22, 1821–1834, 2003.
- Tindale, N.W., Pease, P.P., 1999. Aerosols over the Arabian Sea: Atmospheric transport pathways and concentrations of dust and sea salt. *Deep-Sea Res. II Top. Stud. Oceanogr.* 46 (8–9), 1577–1595.
- Vasilatou, V., Manousakas, M., Gini, M., Diapouli, E., Scoullou, M., & Eleftheriadis, K. (2017). Long term flux of Saharan dust to the Aegean sea around the Attica region, Greece. *Frontiers in Marine Science*, 4, 42.
- Vincent, J., Laurent, B., Losno, R., Bon Nguyen, E., Rouillet, P., Sauvage, S., ... & Bergametti, G. (2016). Variability of mineral dust deposition in the western Mediterranean basin and south-east of France. *Atmospheric Chemistry and Physics*, 16(14), 8749-8766.

Table 1. Aerosol sample name collected during dust storm, the date of collection, aerosol concentration, Al and Fe concentration, dust concentration and dust flux.

	Date of collection	Aerosol concentration	Al	Fe	Dust concentration	Dust percentage	Dust Flux
		($\mu\text{g}/\text{m}^3$)				(%)	$\text{mg m}^{-2} \text{day}^{-1}$
DS-1	05-Mar-12	147	10.61	6.98	132	90	44
DS-2	24-Mar-12	157	7.48	4.11	93	59	31
DS-3	27-Dec-12	111	6.36	5.35	79	71	27
	28-Dec-12	189	9.24	3.90	115	61	39
DS-4	06-Feb-13	184	8.88	3.41	110	60	37
DS-5	10-Apr-13	211	8.96	4.11	111	53	37
DS-6	09-May-13	148	6.0	1.86	74	50	25
	13-May-13	172	9.03	4.12	112	65	38
DS-7	12-15-Jun-13	229	7.58	3.55	94	41	32
DS-8	05-Apr-14	135	6.0	1.84	75	55	25
	06-Apr-14	98	4.7	1.73	59	60	20
	07-Apr-14	125	5.01	2.14	62	50	21
	08-Apr-14	95	5.7	1.83	71	74	24
	10-Apr-14	110	5.01	2.14	62	57	21
DS-9	04-May-14	103	4.96	1.37	62	60	21
DS-10	14-Oct-14	129	4.83	1.69	60	47	20
	15-Oct-14	106	6.0	2.33	74	70	25
	16-Oct-14	80	5.1	2.27	64	80	21
DS-11	07-Apr-15	160	9.29	3.21	116	72	39
	10-Apr-15	117	6.3	1.53	78	67	26
DS-12	25-Apr-15	149	6.44	2.46	80	54	27

Table 2 Samples collected during dry period of 2012-15 and their total concentration. The dust concentration, percentages and flux were also calculated using Al concentration in the samples

Sample ID	Date of collection	Aerosol concentration	Al			Dust concentration	Dust percentage (%)	Dust Flux $\text{mg m}^{-2} \text{day}^{-1}$
			Al	Fe	Ti			
DS-1-1	1-Mar-2012	45	0.91	0.89	0.1	11	25	4
DS-1-2	2-Mar-2012	116	4.90	4.64	0.9	61	53	20
DS-1-3	3-Mar-2012	182	1.54	1.74	0.3	19	11	6
DS-1-4	6-Mar-2012	101	1.27	2.36	0.5	16	16	5
DS-1-5	9-Mar-2012	145	1.11	3.43	0.2	14	10	5
DS-2-6	19-Mar-2012	152	0.75	1.29	0.2	9	6	3
DS-2-7	20-Mar-2012	131	1.01	1.47	0.1	13	10	4
DS-2-8	21-Mar-2012	88	0.84	0.63	0.1	10	12	4
DS-2-9	22-Mar-2012	252	2.09	9.18	1.9	26	10	9
DS-2-10	23-Mar-2012	205	2.01	6.59	1.3	25	12	8
DS-2-11	26-Mar-2012	129	3.40	3.89	0.5	42	33	14
DS-2-12	27-Mar-2012	147	1.99	1.21	0.6	25	17	8
DS-2-13	28-Mar-2012	208	3.32	2.73	0.4	41	20	14
DS-2-14	29-Mar-2012	157	3.04	1.94	0.3	38	24	13
DS-3-15	26-Dec-2012	134	3.40	1.81	0.1	42	32	14
DS-3-17	31-Dec-2012	159	5.2	1.14	0.3	64	41	22
DS-4-18	5-Feb-2013	91	2.8	0.99	0.3	34	38	11
DS-4-19	8-Feb-2013	130	2.1	1.83	0.4	26	20	9
DS-5-20	5-Apr-2013	101	2.8	0.69	0.2	35	34	12
DS-5-21	8-Apr-2013	101	3.6	1.22	0.3	45	44	15
DS-5-22	9-Apr-2013	94	3.2	0.84	0.2	40	43	14
DS-5-23	12-Apr-2013	219	3.4	1.90	0.6	42	19	14
DS-5-24	13-Apr-2013	133	3.5	1.64	0.5	43	33	15
DS-5-25	14-Apr-2013	156	4.1	2.13	0.6	51	33	17

Sample ID	Date of collection	Aerosol concentration	Al Fe Ti			Dust concentration	Dust percentage (%)	Dust Flux mg m ⁻² day ⁻¹
			(µg/m ³)					
DS-5-26	15-Apr-2013	134	3.2	1.65	0.5	39	29	13
DS-6-27	6-May-2013	109	3.3	1.03	0.3	41	38	14
DS-6-28	7-May-2013	102	2.9	1.66	0.5	36	35	12
DS-6-29	8-May-2013	98	3.7	1.67	0.4	45	46	15
DS-8-35	9-Apr-2014	104	3.16	2.44	0.4	39	38	13
DS-8-36	11-Apr-2014	125	3.11	1.91	0.3	39	31	13
DS-8-37	12-Apr-2014	84	2.72	1.42	0.2	34	40	11
DS-8-38	13-Apr-2014	74	2.80	1.72	0.2	35	47	12
DS-9-39	1-May-2014	105	3.6	1.76	0.3	44	42	15
DS-9-40	2-May-2014	95	3.3	2.53	0.4	41	43	14
DS-9-41	3-May-2014	103	2.7	2.42	0.4	33	32	11
DS-9-42	5-May-2014	109	4.1	1.64	0.3	51	47	17
DS-9-43	6-May-2014	135	5.1	1.63	0.2	64	47	21
DS-9-44	7-May-2014	97	3.0	1.19	0.1	38	39	13
DS-10-46	13-Oct-2014	118	4.0	2.29	0.3	50	42	17
DS-11-52	1-Apr-2015	9	0.2	1.40	0.1	3	28	1
DS-11-54	4-Apr-2015	152	3.9	3.96	1.5	49	32	16
DS-11-55	8-Apr-2015	108	3.1	0.97	0.4	38	36	13
DS-11-56	9-Apr-2015	91	3.6	1.37	0.4	45	50	15
DS-12-59	20-Apr-2015	38	1.74	0.30	0.1	22	57	7
DS-12-60	21-Apr-2015	46	1.00	0.11	0.0	12	27	4
DS-12-61	22-Apr-2015	38	1.64	0.34	0.1	20	54	7
DS-12-62	24-Apr-2015	28	1.34	0.29	0.1	17	60	6
DS-12-63	26-Apr-2015	58	1.78	0.48	0.1	22	38	7
DS-12-64	27-Apr-2015	34	0.74	0.31	0.1	9	27	3

Table 3: Samples collected during wet deposition period of 2013-15 and dust flux along with of Al, Fe and Ti percentages are given below

Sample Id	Date of collection	Wet deposition flux (mg m⁻² day⁻¹)	Al %	Fe%	Ti %
WD-13-1	7-10 Jun 2013	678	6.0	4.2	0.4
WD-13-2	11-12 Jun 2013	435	3.9	3.8	0.4
WD-13-3	18-19 Jun 2013	109	5.8	4.2	0.4
WD-13-4	25-26 Jun 2013	195	6.3	5.0	0.6
WD-13-5	29-30 Jun 2013	166	6.6	5.0	0.5
WD-13-6	3-4 Jul 2013	332	7.4	5.2	0.6
WD-13-7	12-13 Jul 2013	379	7.5	5.2	0.6
WD-13-8	18-19 Jul 2013	1019	6.5	5.1	0.5
WD-13-9	23-24 Jul 2013	848	5.5	4.0	0.5
WD-13-10	31 Jul-1 Aug 2013	519	6.1	4.9	0.5
WD-13-11	6-7 Aug 2013	124	5.6	4.2	0.5
WD-13-12	12-13 Aug 2013	141	4.1	3.3	0.3
WD-13-13	17-18 Aug 2013	67	6.2	4.1	0.5
WD-13-14	10-11 Sep 2013	42	5.1	5.5	0.5
WD-13-15	19-20 Sep 2013	127	7.5	4.9	0.5
WD-13-16	28-30 Sep 2013	95	5.9	4.0	0.4

Sample Id	Date of collection	Wet deposition flux (mg m⁻² day⁻¹)	Al %	Fe%	Ti %
WD-14-1	2-3 Jun 2014	98	7.9	5.5	0.6
WD-14-2	14-15 Jun 2014	385	8.2	5.5	0.6
WD-14-3	16-17 Jun 2014	303	8.3	5.7	0.6
WD-14-4	21-26 Jun 2014	581	5.9	4.1	0.4
WD-14-5	8-9 Jul 2014	339	5.1	3.4	0.4
WD-14-6	13-14 Jul 2014	150	7.6	5.5	0.6
WD-14-7	19-20 Jul 2014	389	7.6	5.9	0.7
WD-14-8	22-23 Jul 2014	295	7.6	6.0	0.7
WD-14-9	30-31 Jul 2014	217	8.0	5.0	0.6
WD-14-10	4-5 Aug 2014	341	7.1	5.4	0.6
WD-14-11	7-8 Aug 2014	209	7.3	5.0	0.6
WD-14-12	11-12 Aug 2014	143	7.2	5.2	0.5
WD-14-13	26-27 Aug 2014	56	7.3	4.9	0.5
WD-14-14	4-5 Sep 2014	57	7.6	4.8	0.5
WD-14-15	13-14 Sep 2014	90	7.3	4.9	0.5

Sample Id	Date of collection	Wet deposition flux (mg m⁻² day⁻¹)	Al %	Fe%	Ti %
WD-15-1	24-May-15	101	7.1	6.7	0.7
WD-15-2	20-21 Jun 2015	188	7.6	4.8	0.5
WD-15-3	25-26 Jun 2015	435	7.0	4.6	0.4
WD-15-4	30 Jun-2 Jul 2015	999	9.0	6.5	0.7
WD-15-5	8-9 Jul 2015	494	8.0	5.2	0.6
WD-15-6	15-16 Jul 2015	469	8.1	5.9	0.6
WD-15-7	21-22 Jul 2015	356	8.6	5.5	0.5
WD-15-8	26-27 Jul 2015	73	8.5	5.7	0.6
WD-15-9	31 Jul - 1 Aug 2015	126	8.5	5.9	0.7
WD-15-10	6-7 Aug 2015	218	8.5	6.0	0.7
WD-15-11	12-13 Aug 2015	316	8.3	5.6	0.6
WD-15-12	16-17 Aug 2015	121	8.4	6.0	0.7
WD-15-13	28-30 Aug 2015	413	7.9	5.3	0.6
WD-15-14	12-14 Sep 2015	135	4.5	4.3	0.4
WD-15-15	18-20 Sep 2015	342	7.5	4.6	0.5

Supplementary Material

Assessment of aeolian dust concentration, elemental composition, and their wet and dry deposition fluxes over the Northeast Arabian Sea

Suresh, K.^{1,2}, Udisha Singh^{1,3}, Ashish Kumar Jha⁴, Vishnu Murthy Matta⁵, A.K. Sudheer², Ashwini Kumar^{1,3*}

¹*CSIR-National Institute of Oceanography, Dona Paula, Goa, India*

²*Physical Research Laboratory, Ahmedabad, India*

³*Academy of Scientific and Innovative Research (AcSIR), Ghaziabad, U.P., 201002- India*

⁴*Department of Zoology, Hislop College, Nagpur, 440001, (M.S), India*

⁵*The School of Earth, Ocean and Atmospheric Sciences, Goa University, Taleigao, India*

*Corresponding author:

Ashwini Kumar

Geological Oceanography Division

CSIR-National Institute of Oceanography

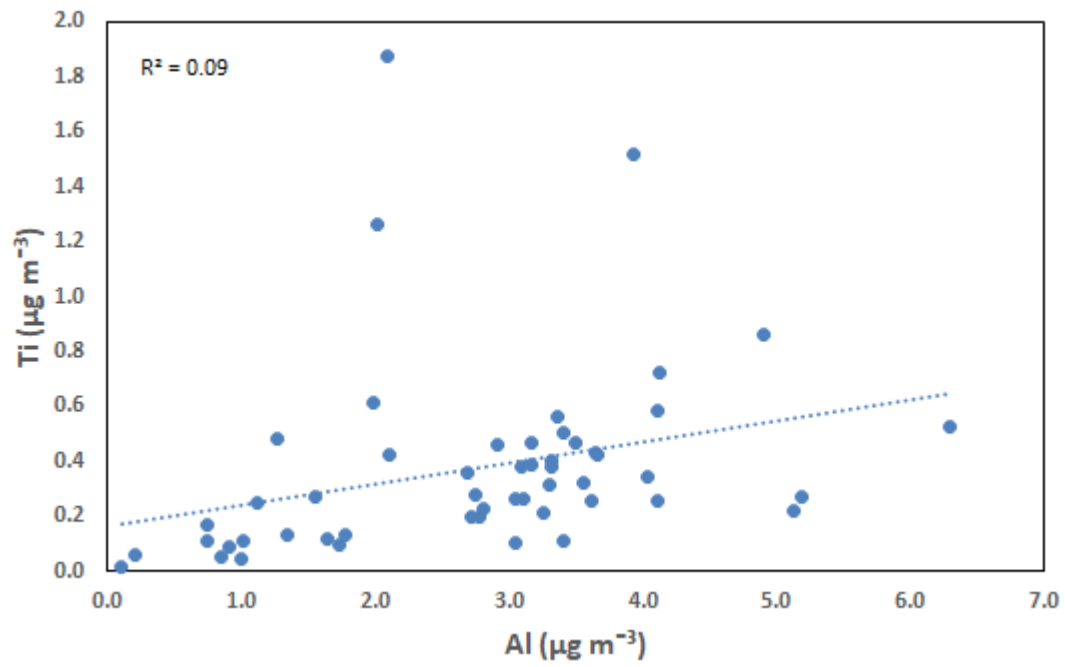
Dona Paula, Goa-403 004, India

E-mail: ashwinikumarjha@gmail.com, ashwinik@nio.org

Tel: +91 832 2450368, Fax: +91 832 2450602

Supplementary material S1

The scatter plot showing correlation analysis of Ti Vs Al for the non-dust storm samples.



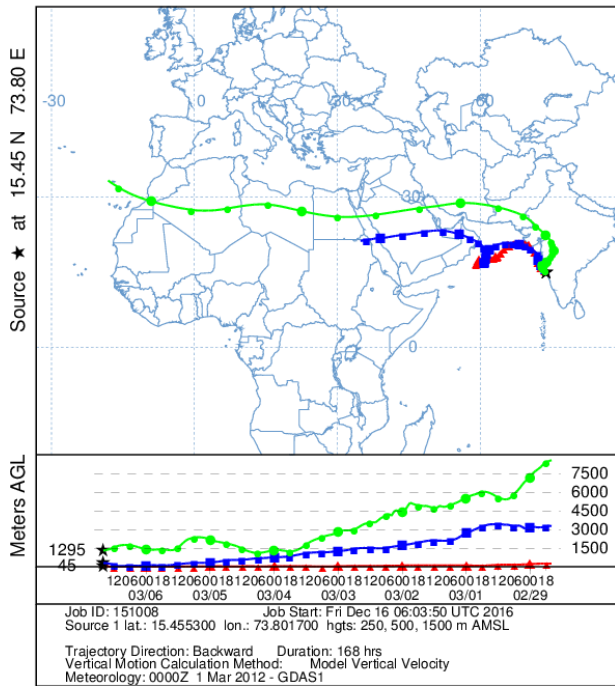
Supplementary material S2

To find the possible source of the mineral dust aerosol, HYBRID Single-Particle Lagrangian Integrated Trajectory (HYSPLIT) (Draxler and Rolph, 2003) with the GDAS meteorological dataset from the National Oceanic and Atmospheric Administration (NOAA) Air Research Laboratory (<http://www.arl.noaa.gov/ready/hysplit4.html>) was used. Backward trajectories were run for the day of sampling for 168 hours at different altitude (mainly 500-3000m) levels above ground level during sampling days, to show the origin of dust laden air mass at different altitudes from different regions.

Dry dust storm samples

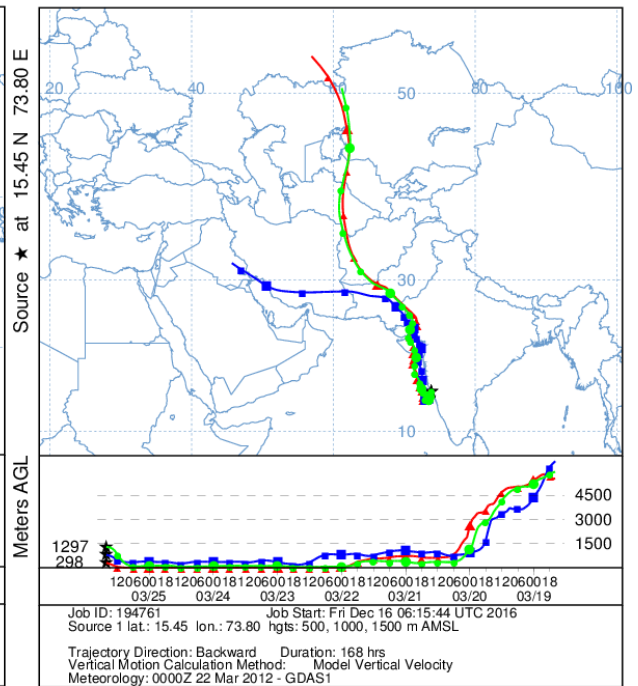
DS-1

NOAA HYSPLIT MODEL
Backward trajectories ending at 1600 UTC 06 Mar 12
GDAS Meteorological Data



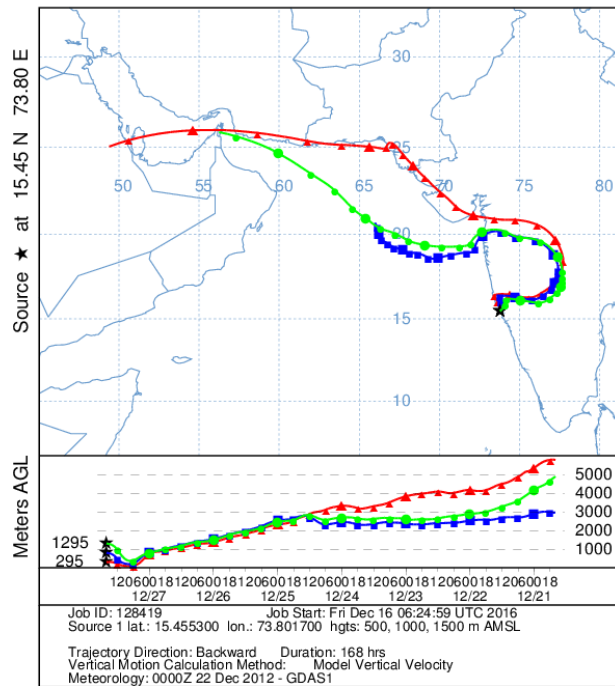
DS-2

NOAA HYSPLIT MODEL
Backward trajectories ending at 1600 UTC 25 Mar 12
GDAS Meteorological Data



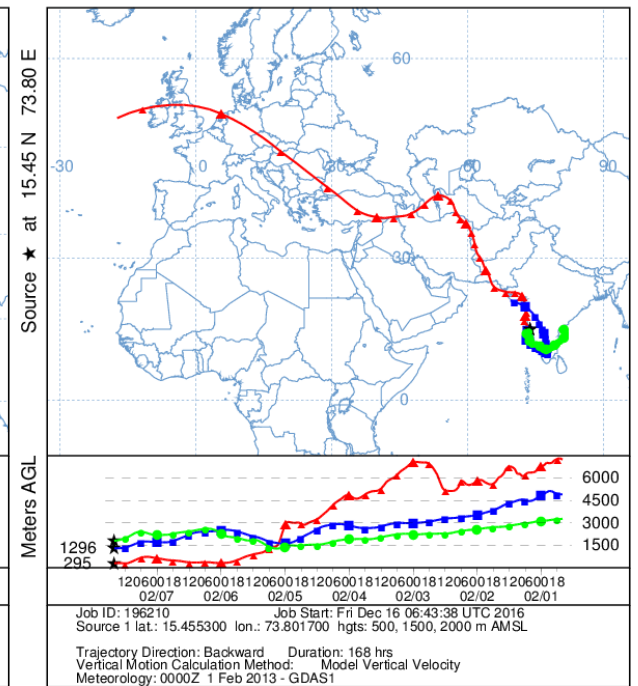
DS-3

NOAA HYSPLIT MODEL
Backward trajectories ending at 1600 UTC 27 Dec 12
GDAS Meteorological Data



DS-4

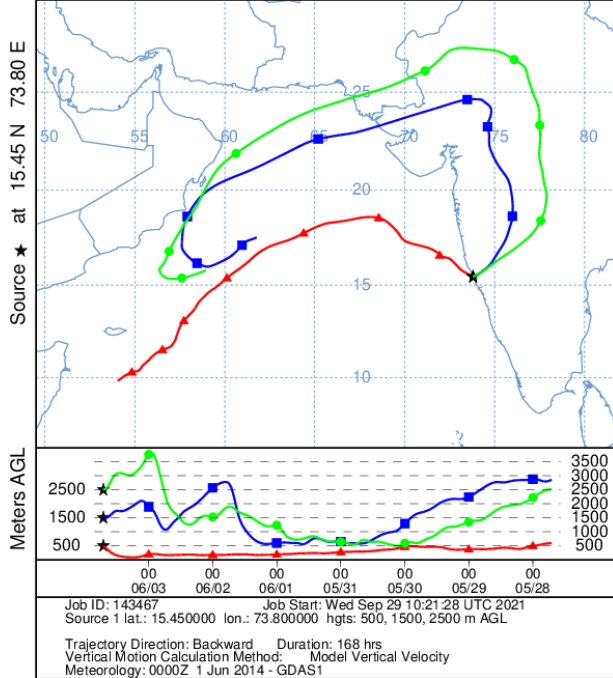
NOAA HYSPLIT MODEL
Backward trajectories ending at 1600 UTC 07 Feb 13
GDAS Meteorological Data



Wet deposition samples of 2014

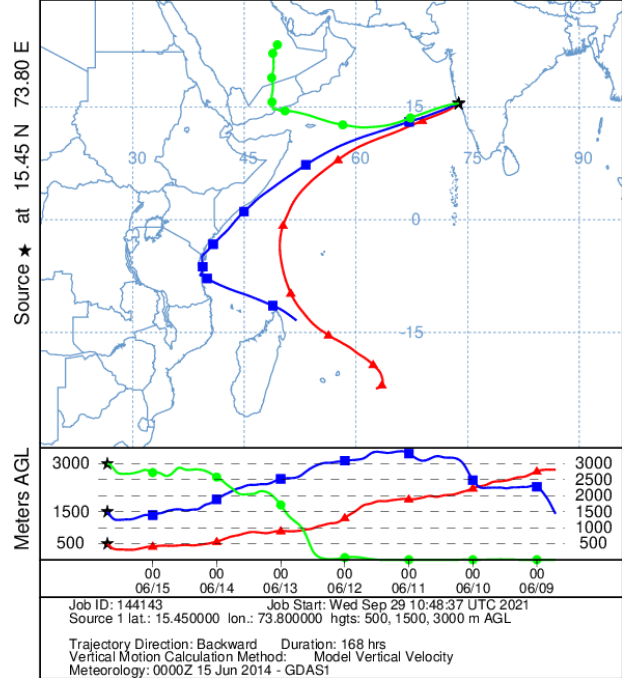
WD-14-1

NOAA HYSPLIT MODEL
Backward trajectories ending at 1700 UTC 03 Jun 14
GDAS Meteorological Data



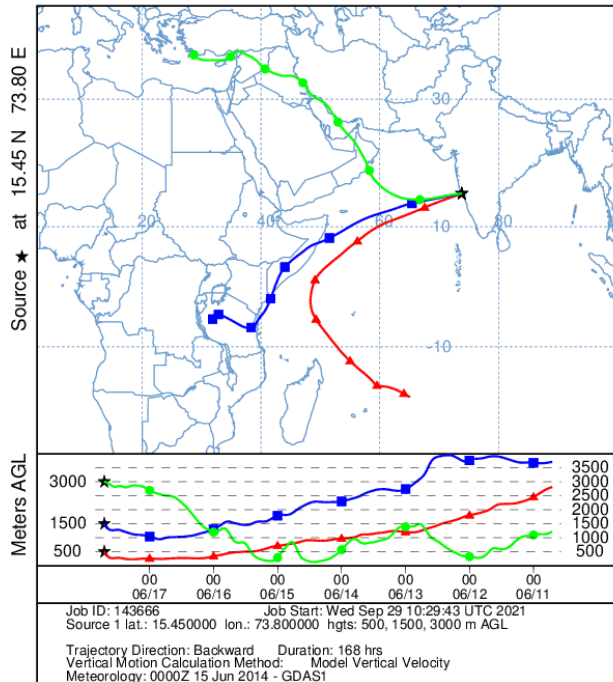
WD-14-2

NOAA HYSPLIT MODEL
Backward trajectories ending at 1700 UTC 15 Jun 14
GDAS Meteorological Data



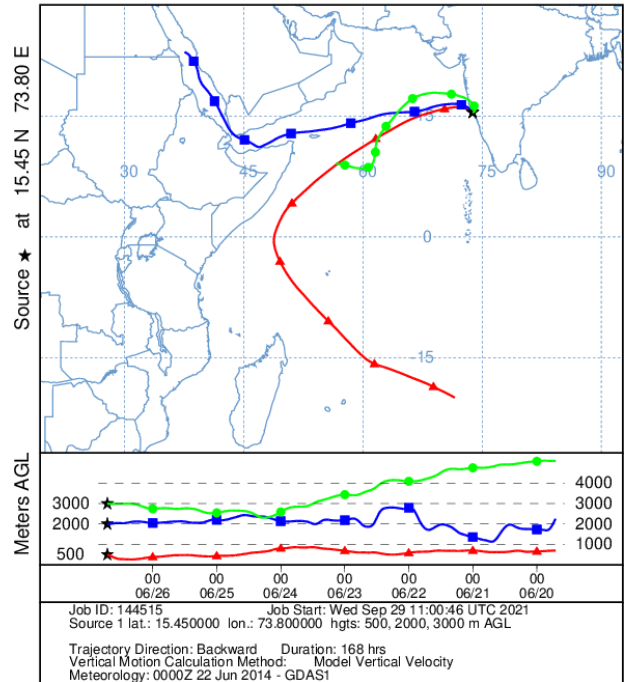
WD-14-3

NOAA HYSPLIT MODEL
Backward trajectories ending at 1700 UTC 17 Jun 14
GDAS Meteorological Data



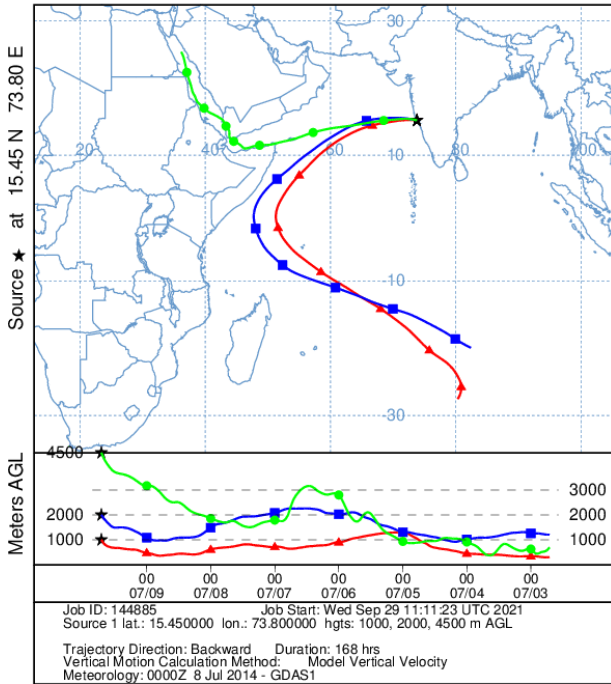
WD-14-4

NOAA HYSPLIT MODEL
Backward trajectories ending at 1700 UTC 26 Jun 14
GDAS Meteorological Data



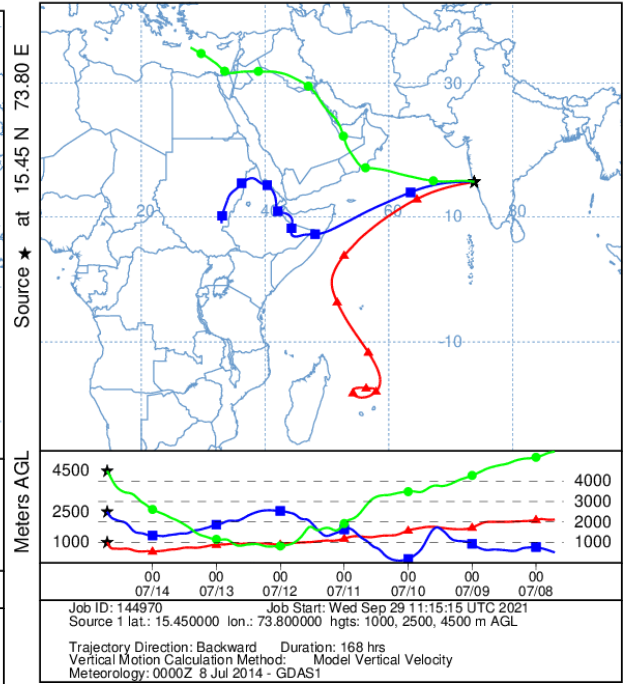
WD-14-5

NOAA HYSPLIT MODEL
Backward trajectories ending at 1700 UTC 09 Jul 14
GDAS Meteorological Data



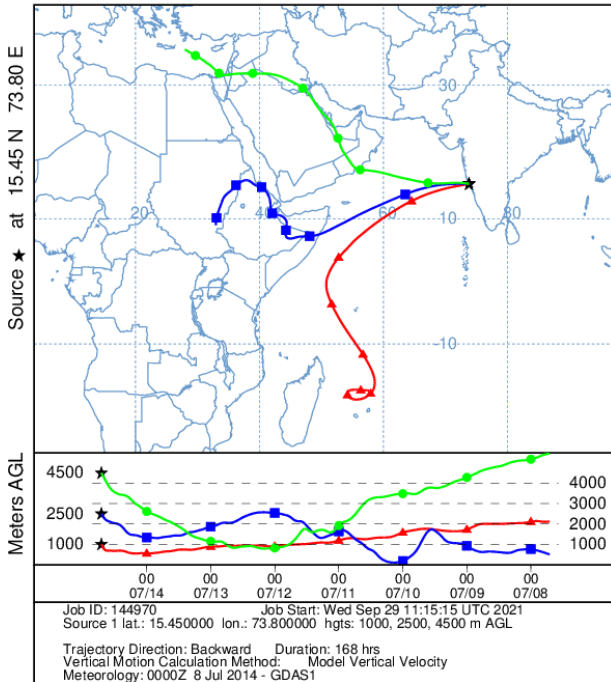
WD-14-6

NOAA HYSPLIT MODEL
Backward trajectories ending at 1700 UTC 14 Jul 14
GDAS Meteorological Data



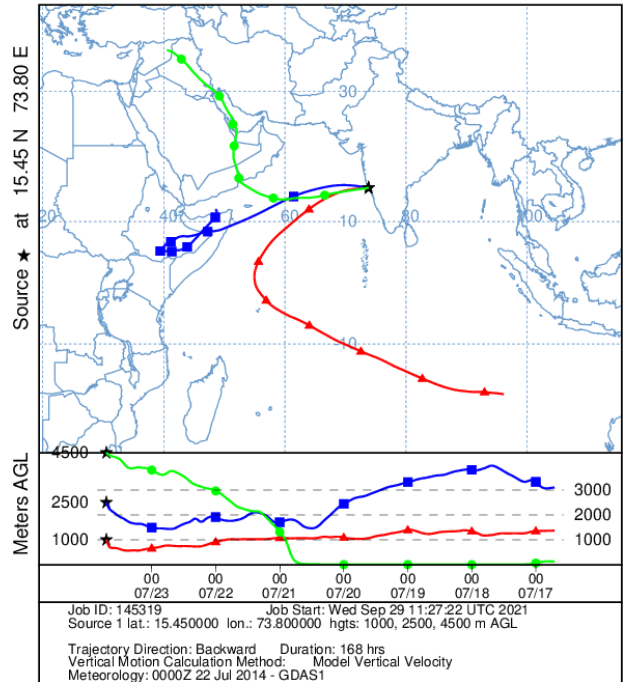
WD-14-7

NOAA HYSPLIT MODEL
Backward trajectories ending at 1700 UTC 14 Jul 14
GDAS Meteorological Data



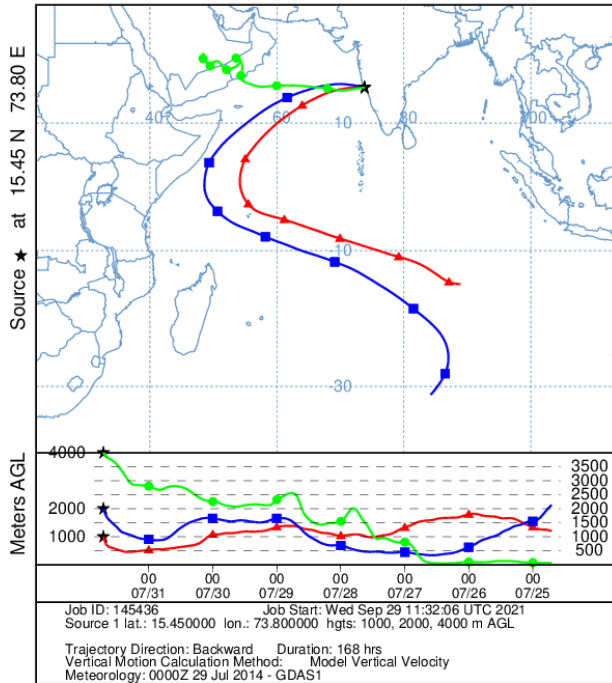
WD-14-8

NOAA HYSPLIT MODEL
Backward trajectories ending at 1700 UTC 23 Jul 14
GDAS Meteorological Data



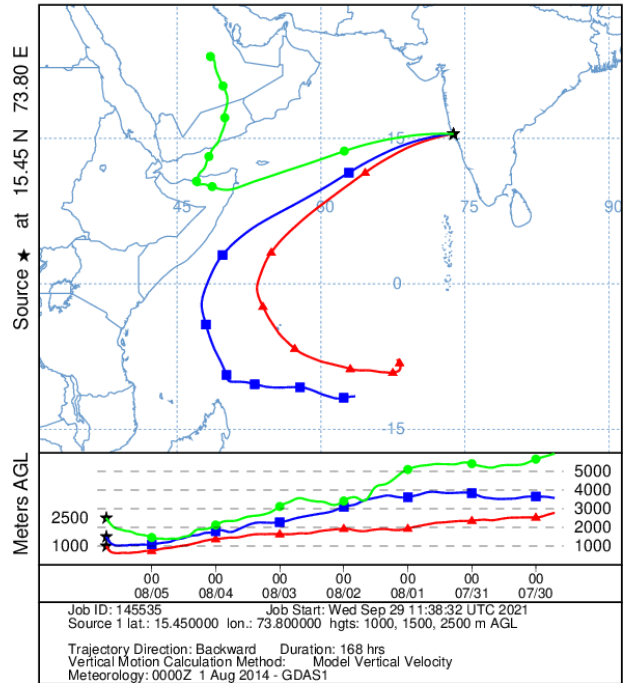
WD-14-9

NOAA HYSPLIT MODEL
Backward trajectories ending at 1700 UTC 31 Jul 14
GDAS Meteorological Data



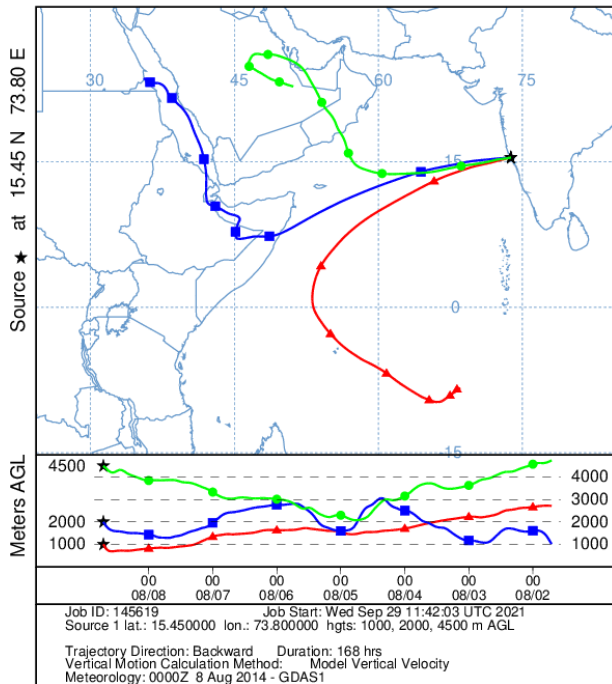
WD-14-10

NOAA HYSPLIT MODEL
Backward trajectories ending at 1700 UTC 05 Aug 14
GDAS Meteorological Data



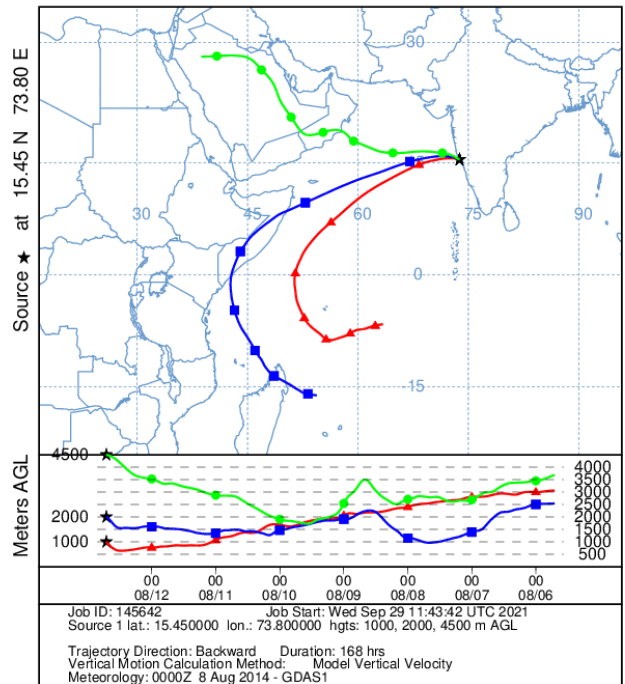
WD-14-11

NOAA HYSPLIT MODEL
Backward trajectories ending at 1700 UTC 08 Aug 14
GDAS Meteorological Data



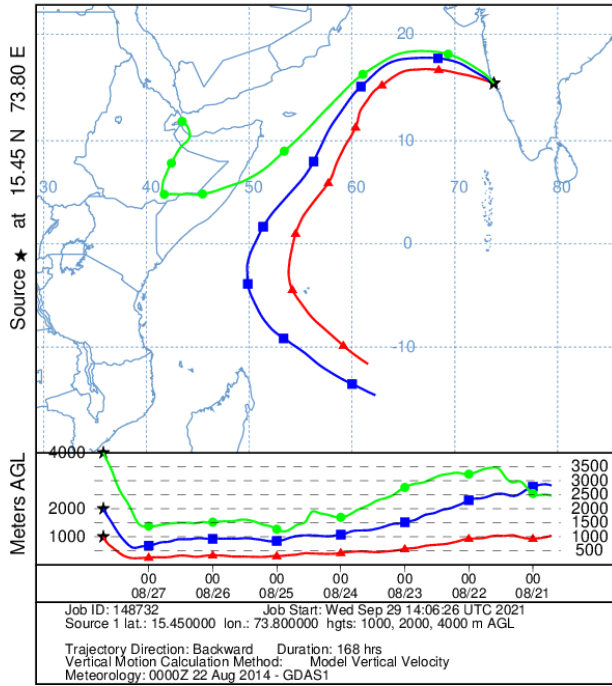
WD-14-12

NOAA HYSPLIT MODEL
Backward trajectories ending at 1700 UTC 12 Aug 14
GDAS Meteorological Data



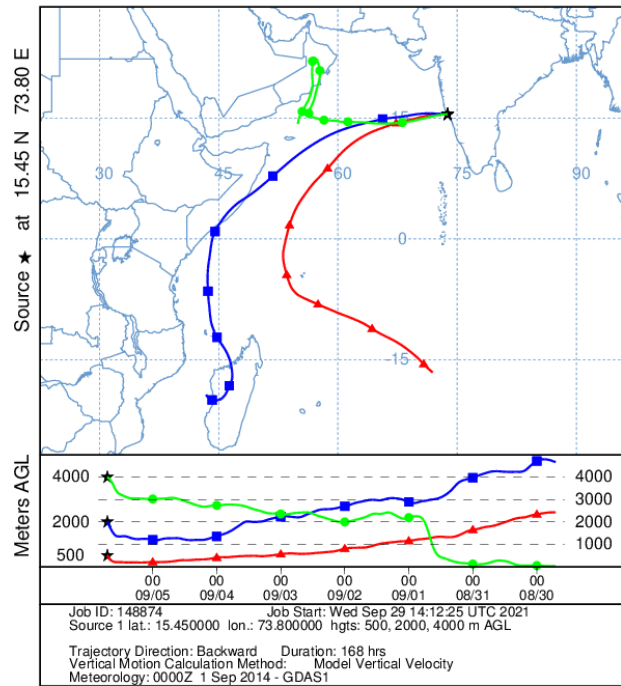
WD-14-13

NOAA HYSPLIT MODEL
Backward trajectories ending at 1700 UTC 27 Aug 14
GDAS Meteorological Data



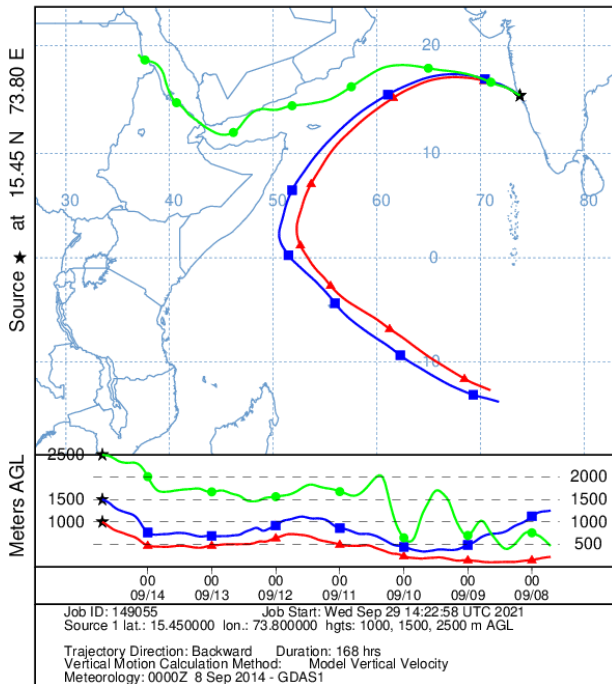
WD-14-14

NOAA HYSPLIT MODEL
Backward trajectories ending at 1700 UTC 05 Sep 14
GDAS Meteorological Data



WD-14-15

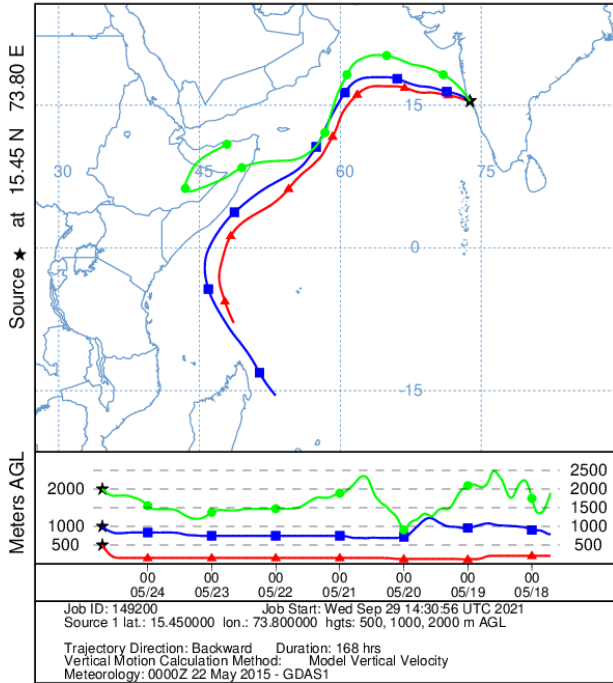
NOAA HYSPLIT MODEL
Backward trajectories ending at 1700 UTC 14 Sep 14
GDAS Meteorological Data



Wet deposition samples of 2015

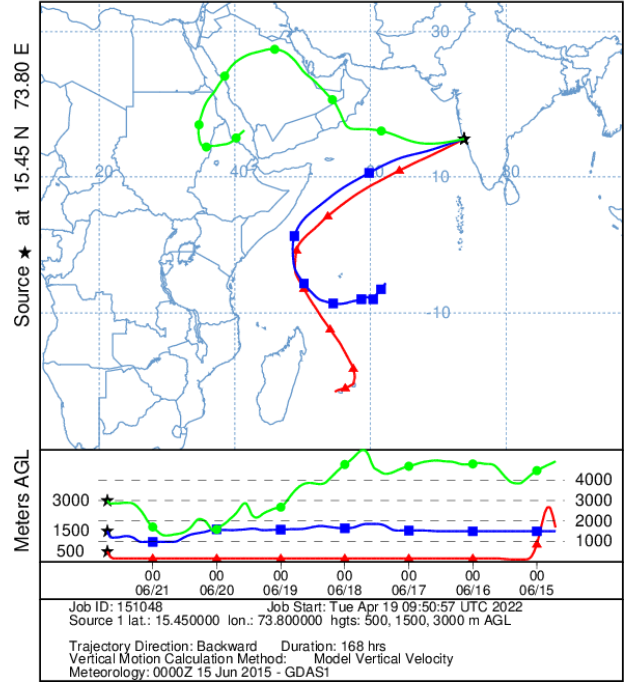
WD-15-1

NOAA HYSPLIT MODEL
Backward trajectories ending at 1700 UTC 24 May 15
GDAS Meteorological Data



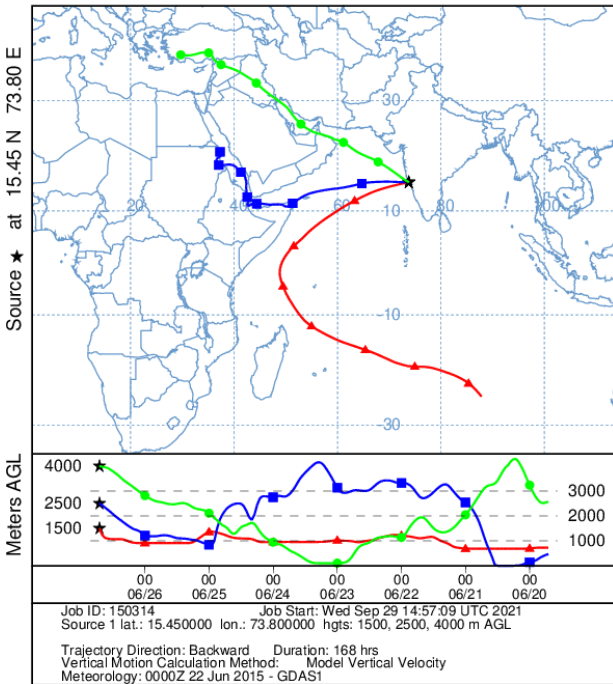
WD-15-2

NOAA HYSPLIT MODEL
Backward trajectories ending at 1700 UTC 21 Jun 15
GDAS Meteorological Data



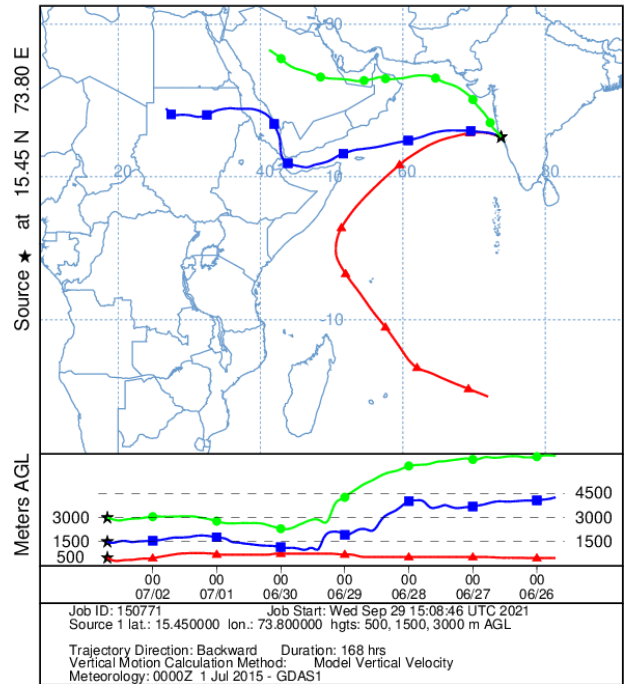
WD-15-3

NOAA HYSPLIT MODEL
Backward trajectories ending at 1700 UTC 26 Jun 15
GDAS Meteorological Data



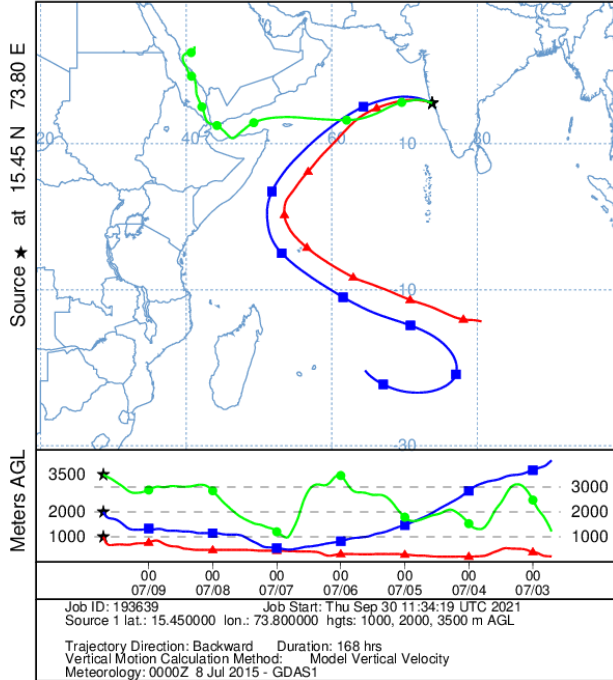
WD-15-4

NOAA HYSPLIT MODEL
Backward trajectories ending at 1700 UTC 02 Jul 15
GDAS Meteorological Data



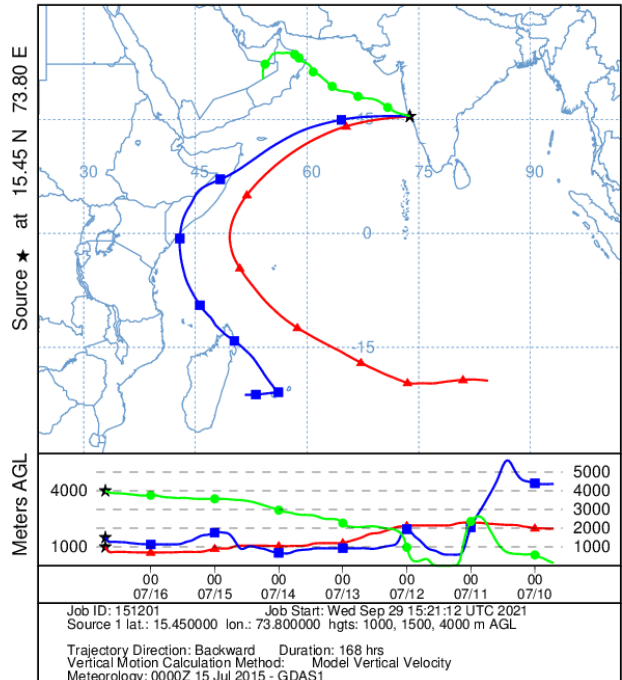
WD-15-5

NOAA HYSPLIT MODEL
Backward trajectories ending at 1700 UTC 09 Jul 15
GDAS Meteorological Data



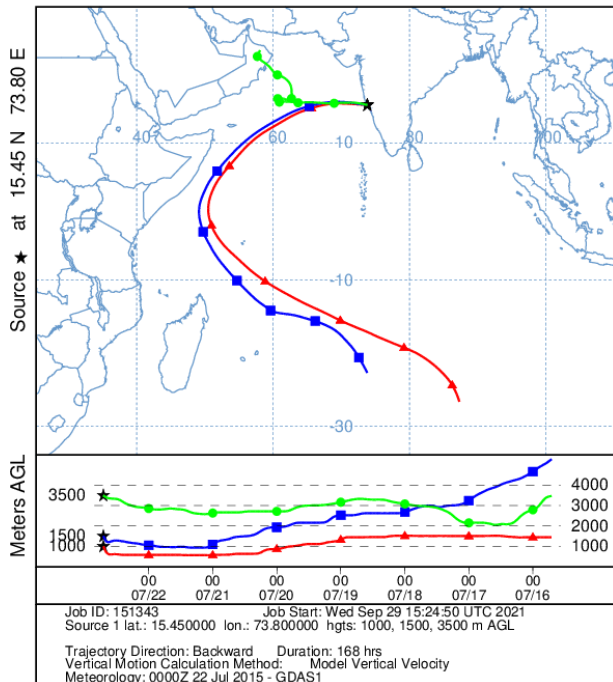
WD-15-6

NOAA HYSPLIT MODEL
Backward trajectories ending at 1700 UTC 16 Jul 15
GDAS Meteorological Data



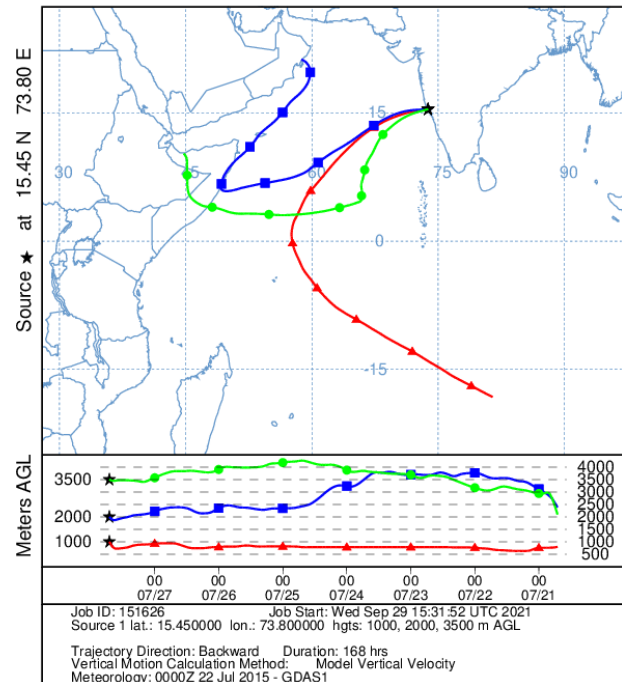
WD-15-7

NOAA HYSPLIT MODEL
Backward trajectories ending at 1700 UTC 22 Jul 15
GDAS Meteorological Data



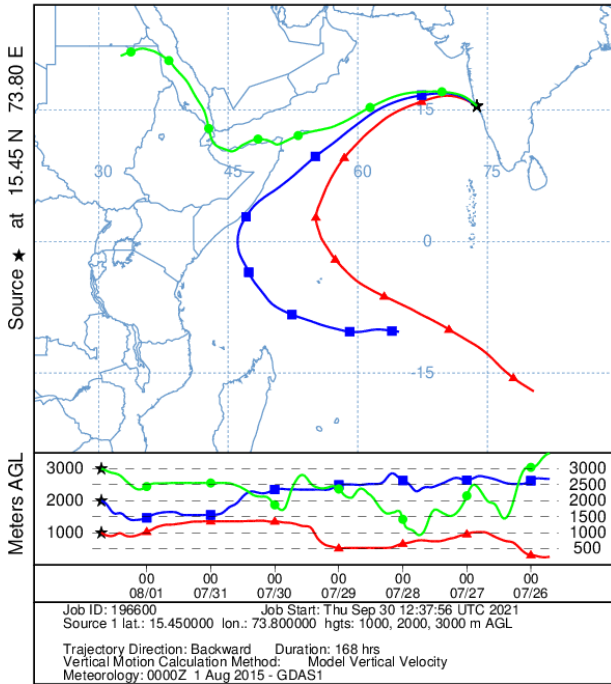
WD-15-8

NOAA HYSPLIT MODEL
Backward trajectories ending at 1700 UTC 27 Jul 15
GDAS Meteorological Data



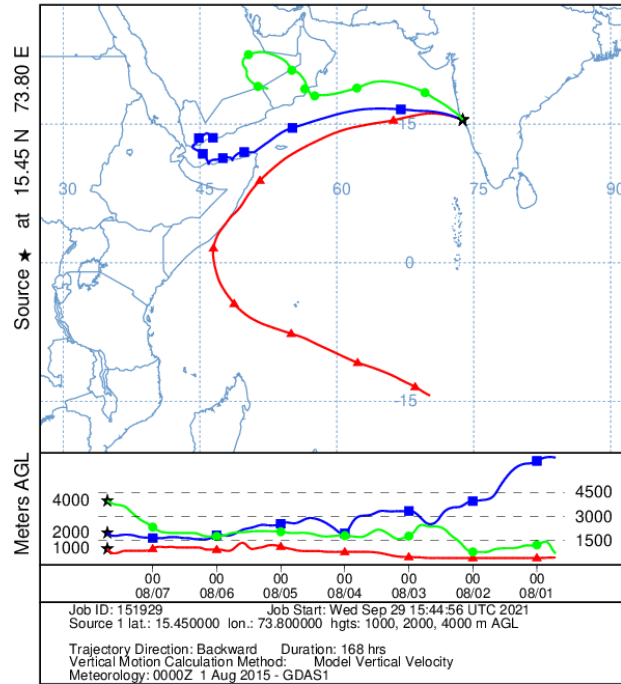
WD-15-9

NOAA HYSPLIT MODEL
Backward trajectories ending at 1700 UTC 01 Aug 15
GDAS Meteorological Data



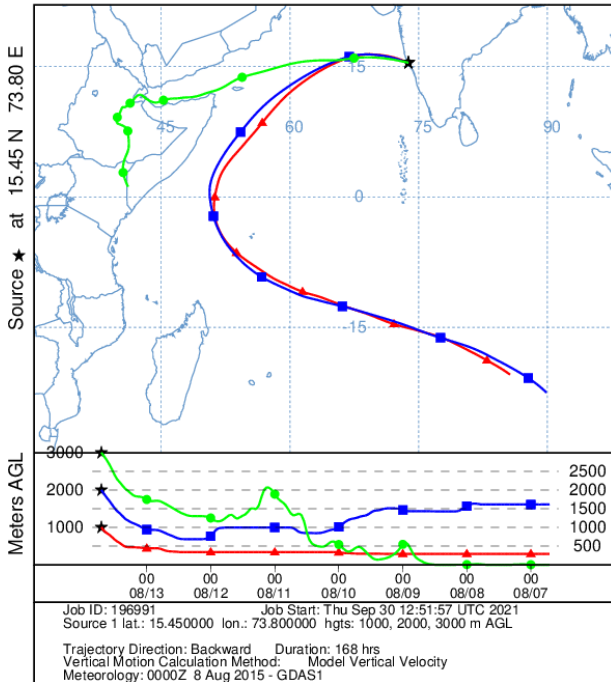
WD-15-10

NOAA HYSPLIT MODEL
Backward trajectories ending at 1700 UTC 07 Aug 15
GDAS Meteorological Data



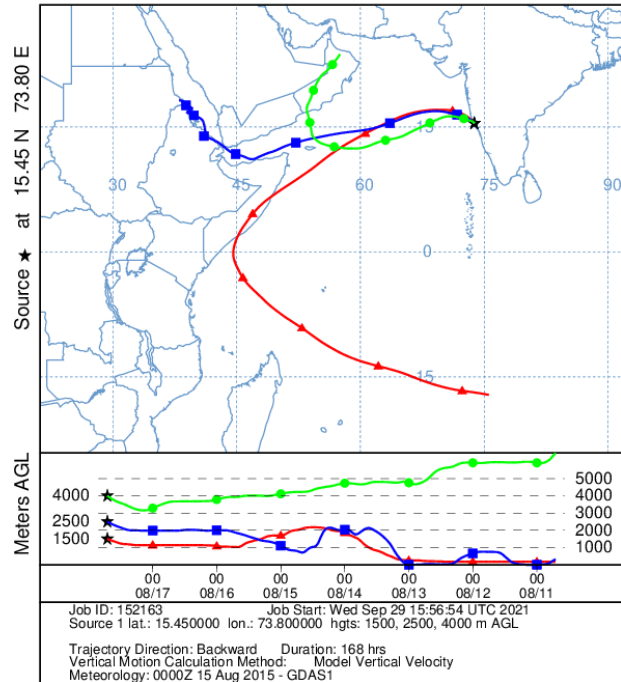
WD-15-11

NOAA HYSPLIT MODEL
Backward trajectories ending at 1700 UTC 13 Aug 15
GDAS Meteorological Data



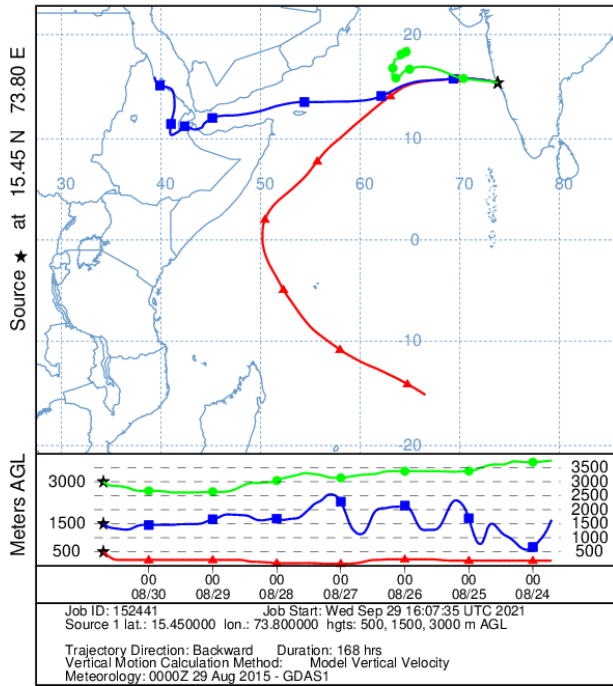
WD-15-12

NOAA HYSPLIT MODEL
Backward trajectories ending at 1700 UTC 17 Aug 15
GDAS Meteorological Data



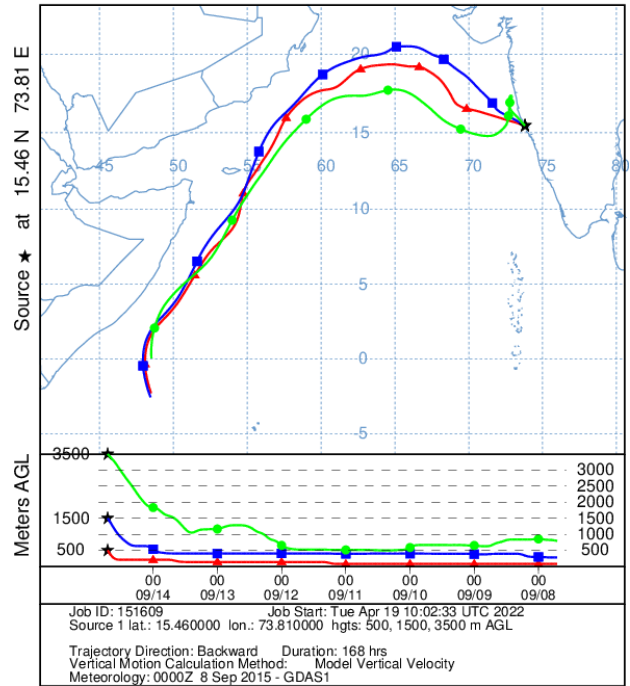
WD-15-13

NOAA HYSPLIT MODEL
 Backward trajectories ending at 1700 UTC 30 Aug 15
 GDAS Meteorological Data

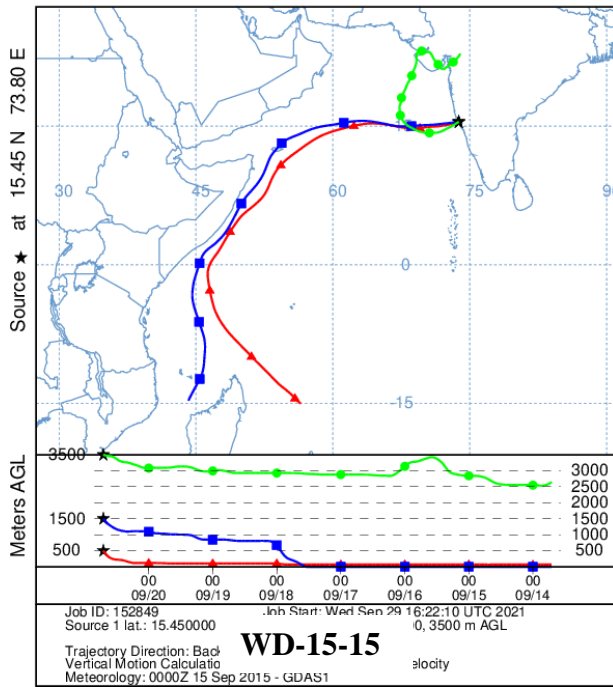


WD-15-14

NOAA HYSPLIT MODEL
 Backward trajectories ending at 1700 UTC 14 Sep 15
 GDAS Meteorological Data



NOAA HYSPLIT MODEL
 Backward trajectories ending at 1700 UTC 20 Sep 15
 GDAS Meteorological Data



WD-15-15